FINAL
CONTRACT REPORT

TESTING OF SELECTED METALLIC REINFORCING BARS FOR EXTENDING THE SERVICE LIFE OF CONCRETE BRIDGES: TESTING IN SOLUTIONS

JOHN R. SCULLY, Ph.D., Professor
CHRISTOPHER A. MARKS, Laboratory Supervisor
MICHAEL F. HURLEY, Graduate Research Assistant

Department of Materials Science and Engineering
University of Virginia

V · I · R · G · I · N · I · A

VTRC

TRANSPORTATION RESEARCH COUNCIL

VIRGINIA TRANSPORTATION RESEARCH COUNCIL

1. Report No. FHWA/VTRC 03-CR11	2. Government Accession No.	3. Recipient's Catalog No.	
4. Title and Subtitle Testing of Selected Metallic Reinforcing Bars For Extending Service Life of Concrete Bridges In Solutions		5. Report Date January 2003	
		6. Performing Organization Code	
7. Author(s) John R. Scully, Ph.D., Christopher A. Marks, and Michael F. Hurley		8. Performing Organization Report No. VTRC 03-CR11	
9. Performing Organization and Address Virginia Transportation Research Council 530 Edgemont Road Charlottesville, VA 22903		10. Work Unit No. (TRAIS)	
		11. Contract or Grant No. 51263	
12. Sponsoring Agencies' Name and Address Virginia Department of Transportation FHWA 1401 E. Broad Street P.O. Box 10249 Richmond, VA 23219 Richmond, VA 23240		13. Type of Report and Period Covered Final Contract Report 1/30/99 – 11/30/02	
		14. Sponsoring Agency Code	
15. Supplementary Notes			

16. Abstract

Stainless steel-clad rebar provides an opportunity to significantly increase the Cl⁻ threshold concentration associated with active corrosion initiation compared to plain carbon steel. However, threshold Cl⁻ concentrations for 316L stainless steel-clad rebar are unknown.   Moreover, the impact of possible galvanic corrosion between the clad layer and any exposed carbon steel core has not been investigated.

The Cl⁻ threshold concentrations for corrosion initiation on clad 316L stainless steel (with a thickness of about 1 mm over a carbon steel core), solid 316LN stainless steel, and plain carbon steel were examined in saturated $Ca(OH)_2$ plus various concentrations of NaCl. The electrochemical properties of "intact" 316L stainless steel-clad rebar were found to be similar to those of solid 316LN stainless steel according to several electrochemical criteria. The Cl⁻ threshold concentrations for corrosion initiation were increased to Cl⁻/OH⁻ molar ratios as high as 17 to 24 even at high anodic potentials for "intact" 316L-clad and solid 316LN stainless steel, respectively. Thus, active corrosion of "intact" 316L-clad rebar could be delayed for many years due to the high Cl⁻/OH⁻ molar ratios required at the stainless steel/concrete interface and the slow transport rate of chloride in concrete. In contrast, the threshold chloride concentration for corrosion initiation on carbon steel was low (Cl⁻/OH⁻ molar ratio < 1.5) at all potentials. Cladding with a physical breech exhibited Cl⁻/OH⁻ thresholds dominated by the exposed plain carbon steel. Galvanic coupling between exposed plain carbon steel and the stainless steel-cladding accelerated corrosion of the plain carbon steel only at and above the Cl⁻/OH⁻ ratio necessary for corrosion initiation on carbon steel.

| 17 Key Words
Reinforced concrete bridges, reinforcing bars, corrosion of reinforcing bars | | 18. Distribution Statement
No restrictions. This document is available to the public through NTIS, Springfield, VA 22161. | |
| 19. Security Classif. (of this report)
Unclassified | 20. Security Classif. (of this page)
Unclassified | 21. No. of Pages
48 | 22. Price |

Form DOT F 1700.7 (8-72)   Reproduction of completed page authorized

FINAL CONTRACT REPORT

TESTING OF SELECTED METALLIC REINFORCING BARS FOR EXTENDING THE SERVICE LIFE OF CONCRETE BRIDGES: TESTING IN SOLUTIONS

John R. Scully, Ph.D.
Professor of Materials Science and Engineering
University of Virginia

Christopher A. Marks
Laboratory Supervisor
Department of Materials Science and Engineering
University of Virginia

Michael F. Hurley
Graduate Research Assistant
Department of Materials Science and Engineering
University of Virginia

Project Manager
Gerardo G. Clemeña, Virginia Transportation Research Council

NOTICE

The project that is the subject of this report was done under contract for the Virginia Department of Transportation, Virginia Transportation Research Council. The contents of this report reflect the views of the authors, who are responsible for the facts and the accuracy of the data presented herein. The contents do not necessarily reflect the official views or policies of the Virginia Department of Transportation, the Commonwealth Transportation Board, or the Federal Highway Administration. This report does not constitute a standard, specification, or regulation.

Each contract report is peer reviewed and accepted for publication by Research Council staff with expertise in related technical areas. Final editing and proofreading of the report are performed by the contractor.

ABSTRACT

Stainless steel-clad rebar provides an opportunity to significantly increase the Cl⁻ threshold concentration associated with active corrosion initiation compared to plain carbon steel. However, threshold Cl⁻ concentrations for 316L stainless steel-clad rebar are unknown. Moreover, the impact of possible galvanic corrosion between the clad layer and any exposed carbon steel core has not been investigated.

The Cl⁻ threshold concentrations for corrosion initiation on clad 316L stainless steel (with a thickness of about 1 mm over a carbon steel core), solid 316LN stainless steel, and plain carbon steel were examined in saturated $Ca(OH)_2$ plus various concentrations of NaCl. The electrochemical properties of "intact" 316L stainless steel-clad rebar were found to be similar to those of solid 316LN stainless steel according to several electrochemical criteria. The Cl⁻ threshold concentrations for corrosion initiation were increased to Cl⁻/OH⁻ molar ratios as high as 17 to 24 even at high anodic potentials for "intact" 316L-clad and solid 316LN stainless steel, respectively. Thus, active corrosion of "intact" 316L-clad rebar could be delayed for many years due to the high Cl⁻/OH⁻ molar ratios required at the stainless steel/concrete interface and the slow transport rate of chloride in concrete. In contrast, the threshold chloride concentration for corrosion initiation on carbon steel was low (Cl⁻/OH⁻ molar ratio < 1.5) at all potentials. Cladding with a physical breech exhibited Cl⁻/OH⁻ thresholds dominated by the exposed plain carbon steel. Galvanic coupling between exposed plain carbon steel and the stainless steel-cladding accelerated corrosion of the plain carbon steel only at and above the Cl⁻/OH⁻ ratio necessary for corrosion initiation on carbon steel.

FINAL CONTRACT REPORT

TESTING OF SELECTED METALLIC REINFORCING BARS FOR EXTENDING THE SERVICE LIFE OF CONCRETE BRIDGES: TESTING IN SOLUTIONS

John R. Scully, Ph.D.
Professor of Materials Science and Engineering
University of Virginia

Christopher A. Marks
Laboratory Supervisor
Department of Materials Science and Engineering
University of Virginia

Michael F. Hurley
Graduate Research Assistant
Department of Materials Science and Engineering
University of Virginia

INTRODUCTION

Corrosion of Carbon Steel Rebar in Concrete

Concrete is approximately 10 times stronger in compression than in tension. Low-cost steel reinforcement, typically AISI/SAE 1040, has been added to greatly increase the composite tensile strength in construction applications (Nawy, 2000). However, the corrosion of concrete reinforcing steel in aggressive environments has been observed for the last 75 years (Tonini and Gaidis, 1980). Loss of rebar cross sectional area, due to corrosion, results in both a lower tensile strength of the structure and corrosion product formation that may damage concrete. Corrosion results in the formation of iron oxides. These oxides occupy a greater volume than the original metal, creating internal tensile stresses in the concrete, and eventually lead to concrete cracking, spalling, and rebar/concrete debonding (Mehta, 1986). This damage exacerbates the corrosion process by creating an easier pathway for oxygen and aggressive ion diffusion to the rebar. In the U.S. alone, over 50% of the bridges in use are affected by corrosion of the reinforcing steel. Of those 50%, approximately 20% are known to be structurally flawed (Participant Workbook, 1985). Costly concrete repairs are often undertaken when non-destructive evaluation indicates extensive cracking (USDOT, 1998). The economic impact of prevention and repair of damage from rebar corrosion is a major motivator behind research on the mitigation of reinforcing steel corrosion.

In the presence of a high-pH concrete pore solution, rebar steel is protected from corrosion by a naturally occurring oxide film (Bentour et al., 1997). Secondary protection may be offered by deposition of mineral scales inherent to the concrete mix (Mehta, 1986). Such protection of rebar provided by concrete is highly dependent on both the properties and quality of the concrete. The quality of the concrete is a function of the initial concrete mix design and greatly affects the resulting permeability and electrical resistance of the concrete (Hausmann, 1967; Feliu et al., 1989).

Permeability of concrete allows for the transport of corrosive elements such as oxygen and chloride from the external environment to the rebar surface. The electrical resistivity of concrete is inversely proportional to permeability of concrete. Low-permeability concrete usually results in longer corrosion initiation times for rebar in concrete since the diffusion time of aggressive ions to the rebar surface is prolonged (Bentour et al., 1997). Electrical resistivities of concrete depend greatly of the degree of concrete hydration and have been measured as high as 10^{11} ohm-cm (oven dried) and as low as 10^3 ohm-cm (saturated). Concrete resistivity gives an indication of the relative ease with which corrosion may occur, since an ionic conducting path is necessary between the anodic and cathodic reaction sites for corrosion to occur. It has been reported that the probability of corrosion initiation decreases, from very likely to unlikely, when the resistivity of the concrete is increased from 6500 ohm-cm to 8500 ohm-cm (Hope and Ip, 1985). The permeability of concrete is a function of the initial water/cement ratio, the degree of concrete hydration, the size and amount of aggregate, and the use of concrete admixtures. Generally, a low water/cement ratio results in a low concrete porosity. A higher degree of porosity results in larger, better-connected, capillary channels in concrete (Mehta, 1986). The amount and size of coarse aggregates also greatly affect concrete permeability. Although aggregates themselves generally have a lower permeability than the surrounding cement, a concrete's porosity is generally enhanced with increasing coarse aggregate content and size (Mehta, 1986). This is because as concrete sets, microcracks (generally larger than the capillaries present in the cement) develop at the transition zone between the coarse aggregate and the cement paste. The maximum coarse aggregate size influences the amount of microcracks present at the aggregate/cement paste interface. On the other hand, the use of more and larger coarse aggregates allows for less paste to be used and can, therefore, reduce the porosity.

The high pH of concrete, generally 12.8 to13.5, allows the formation of a passivating oxide layer on plain carbon steel rebar (Bentour et al, 1997; Mehta, 1986; Hausmann, 1967). However, ferrous and ferric oxides and hydroxides are not protective when the pH is less than about 11.5 (Kurtis and Mehta, 1997) or when sufficient chloride ions are present to destabilize them. In solutions having a moderate pH (approximately 4 to 10), a ferrous oxide forms on the rebar surface, sheltering the underlying metal from the bulk solution, and maintains the local pH around 9.5 (Uhlig and Greene, 1985). The time until carbonation, chloride ingress, or a combination of both leads to depassivation is termed the corrosion initiation stage. Corrosion initiation by carbonation is considered to be a function of the concrete cover and quality only and will not be discussed further. The intrinsic corrosion properties of the rebar determine the exact values of the chloride concentration and pH that are required for initiation. The ensuing active corrosion period is known as the propagation stage (Tuutti, 1982).

The Chloride Threshold for Corrosion Initiation

Mechanisms of Chloride-Induced Corrosion

There is general agreement in the literature that chloride ions lead to depassivation, but the exact mechanism is not well understood. The critical Cl⁻ concentration for corrosion initiation is a useful metric that helps define the time until corrosion initiation. One theory is that dissolved

oxygen predominately favors the γ-FeOOH conversion reaction. Therefore, localized pitting attack caused by sufficient chloride ion concentration will preferentially occur at regions of low dissolved oxygen content (Bentour and Diamond, 1997). The initial oxide film formed on steel in concrete is Fe(OH)$_2$, which is then converted to either ferrous (Fe^{2+}) or ferric (Fe^{3+}) oxide (also known as γ-FeOOH) (Bentour and Diamond, 1997). Although γ-FeOOH is the more stable of the two oxides, it forms more slowly. Because these conversions are never complete, chloride ions may compete with the conversion of Fe(OH)$_2$ to γ-FeOOH by the following reaction:

$$Fe(OH)_2 + 6Cl^- \leftrightarrow FeCl_6^{-3} + 2OH^- + e^- \tag{1}$$
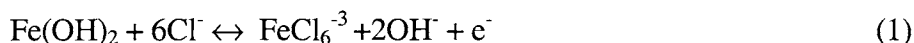
The chloride complex formed in Equation 1 is soluble in the surrounding pore solution and, therefore, does not provide protection against corrosion of the rebar surface. Pore solutions containing sufficient chloride concentrations will promote localized areas of depassivation on the rebar surface where the ferrous oxide has not been converted to γ-FeOOH, even if the pore solution pH is above 11.5.

However, the exact mechanism of breakdown likely differs in the case of a Cr-containing stainless steel passivated with Cr$_2$O$_3$ or CrOOH. According to the adsorption theory of passivity, the Cr-rich passive film becomes unstable when chloride ions replace oxygen ions held within the passive film, causing a difference in electrochemical potential across the film (Rosenberg et al., 1989). According to the oxide film theory, the Cr-rich oxide layer has inherent defects and pores. Chloride ions penetrate the oxide layer at these defects due to dissolution of the more reactive species in the oxide layer (Kurtis and Mehta, 1997). These latter two theories are most applicable to stainless steel with a bound chromium-rich iron oxide. Chloride adsorption, oxide penetration, and interference with oxide formation are promoted by raising the electrochemical potential. Regardless of mechanism, corrosion initiation is a localized phenomenon caused by a sufficient concentration of chloride ions. The critical chloride content or chloride threshold concentration is the concentration of Cl$^-$ ions that is sufficient to cause active corrosion or induce pitting given enough time. The chloride threshold is unknown for 316L-clad stainless steel.

For localized corrosion initiation on corrosion-resistant materials like stainless steels, the threshold potential for pitting and/or crevice corrosion, E_{thres}, has been found to follow the relationship:

$$E_{thres} = A - B \log[Cl^-] \tag{2}$$

where A and B are constants. The value of B for stainless steel is reported to be between –0.15 and –0.1 V/decade, depending on temperature (Sedriks, 1996). The critical amount of chloride ions that causes local active corrosion is known as the threshold chloride concentration. Thus, higher oxygen levels in conjunction with high chloride would be detrimental because dissolved oxygen (O$_2$) also raises the open circuit potential (OCP) associated with corrosion. Initiation occurs once sufficient chloride ion accumulation has depressed the critical pitting potential of the passive steel rebar to below its OCP (Li and Sagues, 1999). Therefore, the threshold chloride concentration could be interpreted as the chloride level when E_{thres} drops to E_{ocp}. In the high-pH concrete pore solutions,

3

other anions that affect the behavior of E_{thres}, must also be considered in determination of such a threshold potential. E_{thres} in concrete is described more accurately as (Kehler et al., 2001):

$$E_{thres} = A - B \, \log(Cl^- / \Sigma[SO_4^{2-} + OH^- + \text{other anions}]) \qquad (3)$$

This is because migration of these other "benign" anions partially offsets the damaging effects of chloride. Therefore, the molar ratio Cl^-/OH^- should always be the method used for expressing the Cl^- concentration in concrete. A second threshold potential (E_r) exists, below which active local corrosion sites repassivate. E_r is also a function of Cl^- concentration, indicating a Cl^- content, below which repassivation is favored. This potential defines a chloride threshold for corrosion suppression. These threshold potentials are unknown for 316L-clad stainless steel in a concrete pore solution containing chloride.

Defining the Active Corrosion State

From a practical standpoint, defining the transition from passive to active corrosion requires that the conditions favoring depassivation remain over time. Because of this, certain definitions of active corrosion are less reliable. Observation of the formation of oxides by visual inspection may not necessarily indicate steady-state active corrosion or, conversely, significant accumulation of oxides may not occur until some time after the shift to active corrosion. Likewise, during OCP monitoring, a shift in E_{OCP} may not be detected upon depassivation or may not necessarily mean significant depassivation, depending on experimental test conditions.

Although it is generally agreed that a unique critical concentration of chloride ions that leads to depassivation exists, there is little agreement on an exact quantitative amount of chloride required for depassivating plain carbon steel. The concentration of chloride that causes depassivation depends heavily on other variables such as oxygen concentration, pH, rebar surface conditions, presence of other ions in the pore solution, and various concrete properties including type of aggregate, concrete additives, mix design, moisture level, and air content. Chloride threshold values published in the literature are generally based upon tests conducted in one of three experimental setups: rebar cast in concrete, rebar cast in mortar specimens, and rebar in synthetic pore solution(s). The experimental method chosen has led to different expressions for the chloride threshold content.

Results from tests conducted in concrete or mortar are commonly presented as the mass of chloride relative to the mass or volume of concrete, i.e. [kg Cl^-] / [m^3 or kg (concrete)]. This is a relatively simple way to express Cl^- concentration in concrete, and it has been documented in standards (ASTM, 1983; BS 1881, 1988). Despite the ease of using this method, it may not be adequate for all chloride threshold data since not all of the chloride is necessarily available to promote corrosion. Soluble Cl^- is usually the culprit in global depassivation of carbon steels. Presenting the data simply as the mass of chloride over the mass or volume of concrete can be misleading due to inherently uncontrollable variables when working with concrete. For example, the influences of bound chloride, precipitated calcium hydroxide, and concrete water content have

4

been the subject of some debate (Zimmerman et al., 1999; Glass and Buenfield, 2000; Glass et al., 1997).

Chloride binding is the interaction between porous concrete and chloride ions that results in their effective removal from the pore solution. A portion of the chloride present in the concrete mix always becomes bound. One important variable concerning the amount of chloride binding that occurs is the tricalcium aluminate (C_3A) content of the cement (Glass and Buenfield, 2000). A greater amount of chloride becomes bound with increasing C_3A content. This occurs by the formation of a relatively insoluble hydration compound called Friedel's salt ($C_3A \cdot CaCl_2 \cdot 15H_2O$) (Kurtis and Mehta, 1997). Other factors including silica fume, granulated blast furnace slag cement replacement, pore solution pH, cation of the chloride salt, and the water/cement ratio also affect the chloride binding capacity (Glass and Buenfield, 1997). The effect of chloride binding on the chloride threshold is unresolved.

Chloride threshold results have also been presented as free chloride (chloride ion concentration in pore solution, only) or as a chloride (soluble) to hydroxyl ion ratio (Alonso et al., 2000). Presentation of data via these two approaches takes into account the hypothesis that only unbound chloride ions contribute to the corrosion activity of steel in concrete. However, presenting the data this way does not decrease the range of chloride threshold values presented. In some cases the spread is actually greater (Glass, 2000; Glass and Buenfield, 1997). One possible explanation is the effect of the water/cement ratio on chloride binding behavior. As the water/cement ratio (w/c) decreases, free chloride content increases in a non-linear manner. Also, the resistivity of the concrete and the amount of precipitated $Ca(OH)_2$ may be affected by a change in moisture content (Mehta, 1986; Kurtis and Mehta, 1997). Both of these properties affect the corrosion behavior of the rebar and, therefore, the chloride threshold.

Chloride threshold tests for carbon steel bars studied in synthetic pore solutions show less variability than the other test methods, possibly due to the elimination of many variables associated with the concrete matrix and the concrete/rebar interface. Greater control is gained over the Cl^-/OH^- molar ratio. However, the results from simulated pore solution tests are more conservative than tests done in concrete (Yonezawa, 1998). Part of the difference between solution and concrete testing can be attributed to the presence of solid $Ca(OH)_2$ crystals at the steel/concrete interface. $Ca(OH)_2$ crystals can act as a pH buffer. Dissolution of $Ca(OH)_2$ crystals during active corrosion has been observed (Yonezawa, 1998). The $Ca(OH)_2$ crystals provide an alkali reservoir that can maintain a high pH, keeping the rebar in the passive range. Kurtis and Mehta (1997) argue that mineral scales in concrete improve passivity and thus raise the chloride threshold when tests are conducted in concrete. Although testing in simulated pore solutions may provide results that are more precise than in concrete or mortars, they are more conservative.

Survey of Existing Methods for Chloride Threshold Determination

Several methods exist for determining the threshold chloride concentrations to initiate corrosion. However, agreement between threshold chloride contents determined by different methods has not been accomplished, and not all methods are applicable to all materials. For

example, a common method for chloride threshold determination on plain carbon steel is electrochemical impedance spectroscopy (EIS) at OCP for determination of the polarization resistance, R_p, as a function of chloride. The R_p value is inversely proportional to the corrosion rate and, consequently, can be used to describe the corrosion behavior of the rebar, defining it as active or passive (Jones, 1996). However, this may not be a viable method for stainless steel due to extended test duration; NaCl saturation of the test electrolyte prior to passivity breakdown; or uncertainty in the actively corroding area, which must be known to determine R_p. It may be possible to determine R_p for stainless steel under anodic polarization at +200 mV (a conservative upper bound for the OCP of stainless steel in concrete), as suggested by Bertolini et al. (1996).

Potentiodynamic scans of stainless steel, particularly at high scan rates, can show high apparent threshold potentials that may or may not be associated with passivity breakdown and the onset of local corrosion, even in the presence of crevices and chloride (Thompson and Syrett, 1992; Burstein, 1996). For instance, onset of O_2 evolution may occur prior to pitting or crevice attack. Therefore caution must be used when using potentiodynamic methods to study stainless steel rebar. The most conservative threshold stabilization potentials determined by slow upward scans, potential holds, or upward steps were found to equal the repassivation potential, E_r, determined by potential step down. The E_r is a threshold potential that when exceeded allows pits and crevices to continue to grow. However, pits and crevices will repassivate at potentials below E_r. This is a more reliable indicator of long-term localized corrosion threshold potentials associated with stable crevicing or pitting propagation. It has been suggested that this repassivation potential depends on pit size (Thompson and Syrett, 1992; Dunn and Sridhar, 1995). More recently, however, the dependency of E_r on the amount of corrosion damage has been questioned in the case of crevice corrosion. It appears that the crevice dimensions control mass transport rather than the depth of crevice attack (Kehler et al., 2001). The crevice repassivation potential (E_r) is the recognized, reproducible, localized corrosion threshold potential that is independent of scan rate, electrode area, exposure time, and oxide film thickness. By systematically stepping down the potential after crevice corrosion has been initiated and propagated for a brief period, the repassivation potential (E_r) can be observed, circumventing the problem caused by the semi-stochastic crevice initiation stage of attack (Shibata and Takeyama, 1977). To date, conservative E_r methods have not been applied to stainless steel rebar.

Survey of Existing Data for Chloride Initiation Thresholds Pertinent to Concrete

A summary of chloride threshold results for carbon steel and stainless steel in all three of the common chloride threshold test environments and using a variety of test methods is presented in Tables 1 and 2.

Table 1. Survey of existing data for the chloride threshold concentration to initiate active corrosion on carbon steel rebar (% wc = percent by weight of cement; Cl⁻/OH⁻ molar ratio). After Glass and Buenfield (1997) and Alonso et al. (2000).

Carbon Steel (Conditions)	Reference	Environment	Threshold Values or Ranges			Depassivation detection method
			Free Cl⁻ (% wc)	Total Cl⁻ (% wc)	Cl⁻/OH⁻	
Solutions simulating concrete	(Hausmann, 1967)	Solution			0.60	Shift in E_{corr}
Solutions simulating concrete	(Gouda and Halka, 1970)	Solution			0.35	Anodic polarization, shift in E_{corr}, visual inspection
Steel in alkaline solutions with chlorides	(Goni and Andrade, 1990)	Solution			0.25-0.8	Avg. corrosion rate
Mortar suspensions	(Gouda and Halka, 1970)	OPC BFSC	2.42 1.21			Anodic polarization
Cements with high or low alkali content	(Petterson, 1992; 1994; 1996)	Mortars 80% RH 100% RH	0.6-1.8 0.5-1.7		1.7-2.6 1.7-2.6	Corrosion rate
Brit. OPC and Sp. BFSC (Cl⁻ added as admixture)	(Andrade, 1986)	OPC BFSC			0.15-0.69 0.12-0.44	Corrosion rate
Three OPC mortar (external chloride)	(Hansson and Sorensen, 1988)	100% RH 50% RH	0.6-1.4			Corrosion rate, potentiostatic
Concrete slabs stored in 10% seawater	(Petterson, 1992; 1994; 1996)	Concrete			1.8-2.9	Corrosion rate
Concrete (external chloride)	(Lambert et al., 1991)	Concrete			3.0	Corrosion rate
Concrete with added Cl⁻	(Gouda and Halaka, 1970)	OPC BFSC	3.04 1.01			Anodic polarization
No pre-cleaning bars	(Gouda and Halaka, 1970)	OPC	0.6			Anodic polarization

Cl⁻ added as admixture
  Med. strength concrete
  High strength concrete
  High strength concrete + supplement
  High strength concrete + supplement + fly ash
	(Kayyali and Hague, 1995)	Concrete	1.15
			0.85
			0.80
			0.45
						Assuming threshold Cl⁻ /OH⁻ = 0.6

Carbon Steel (Conditions)	Reference	Environment	Free Cl⁻ (% wc)	Total Cl⁻ (% wc)	Cl⁻/OH⁻	Depassivation detection method
Cement with different C₃A content C₃A = 2.43% C₃A = 7.59% C₃A = 14.00%	(Hussain et al., 1995)	Concrete	 0.14 0.17 0.22	 0.35 0.62 1.0		Assuming threshold Cl⁻/OH⁻ = 0.3
Concrete with admixed Cl⁻ and externally exposed to Cl⁻	(Schiessl and Breit, 1996)			0.5-1 1-1.5		Macrocell currents
Concrete prisms at marine exposure	(Thomas et al., 1990)	Concrete		0.5		Visual observation, mass loss
Reinforced concrete prisms with fly ash at marine exposure Fly ash = 0% Fly ash = 15% Fly ash = 30% Fly ash = 50%	(Thomas, 1996)	Concrete		 0.70 0.65 0.50 0.20		Mass loss
Concrete slabs with added Cl⁻ to various exposure conditions	(Hope and Ip, 1987)	OPC		0.1-0.19		Corrosion rate, visual inspection, mass loss
Simulated pore solution	(Li and Sagues, 2001)	pH 12.6 pH 13.5			0.25-0.7 1.05-1.25	Shift in E_corr, polarization resistance
Simulated pore solution and mortars	(Alonso et al., 2000)	Solution Mortars	 1.24-3.08	 0.39-1.16	0.25-0.8 1.17-3.98	Various

OPC = ordinary portland cement, BFSC = blast furnace slag cement, RH = relative humidity

Table 2. Summary of reported chloride threshold values for solid stainless steel rebar.

Stainless Steel (Conditions)	Reference	Environment	Free Cl⁻ (% wc)	Total Cl⁻ (% wc)	Cl⁻/OH⁻	Depassivation detection method
Concrete prisms 302, 315, 316 bar	(Cox and Oldfield, 1996)	Concrete	> 3.2%			Visual inspection after 22 years showed no signs of active corrosion
Ca(OH)₂ based pore solutions 304, 304L, 316, 316L	(Bertolini et al., 1996)	pH 9 pH 12.6 pH 13.9			1-4 > 2 > 8	Corrosion rate, potentiostatic hold at +200 mV (vs. SCE)

8

The results for carbon steel generally agree that the Cl^-/OH^- molar ratio threshold is less than 1 for solution tests, and some results suggest the threshold is less than 4 in concrete. However, stainless steel exposed at OCP in chloride-contaminated concrete showed no signs of active corrosion after 22 years, and results in solution tests show a Cl^-/OH^- molar ratio threshold greater than 8. Stainless steel also exhibited a higher chloride threshold as the pH was raised. However, little is known about chloride thresholds for clad stainless steel or solid stainless steel tested in a simulated pore solution at a pH of 12.6 or greater.

Alternative Rebar Types

Epoxy-Coated Rebar

Epoxy-coated rebar is desirable from a corrosion standpoint because it provides both a physical barrier between the rebar and aggressive ions and electrical insulation. Although epoxy-coated bars have performed well in laboratory tests, their reported effectiveness in construction applications has been mixed (USDOT, 1998). Coatings in good condition serve as an effective barrier against chloride-induced corrosion. However, the weakness of the coating lies in its susceptibility to mechanical or chemical damage resulting from improper handling or exposure to ultraviolet rays during storage, transport, or placement of the rebar. Epoxy-coated rebar has been ineffective in concrete constantly exposed to tropical seawater (Smith et al., 1993). In contrast it was generally effective in inland concrete exposed only to deicing salts (Smith et al., 1993; Allen, 1993; Sohanghpurwala and Scannell, 1998), despite some reports of problems (Clear, 1996). Undamaged epoxy coatings usually have a thickness in the range of 130 μm to 300 μm, which allows for flexibility without cracking and protection from aggressive ions (Bentour et al., 1997). However, holidays or pinholes in the epoxy coating may create a super aggressive corrosion environment due to the crevicing conditions present at the epoxy/rebar interface. This can lead to epoxy debondment from the rebar by underpaint corrosion processes, which negatively impacts the structural performance of the rebar (Bentour et al., 1997). Also, the epoxy coating may be poorly bonded at the rebar-concrete interface, which detrimentally impacts the load bearing capacity of the reinforced concrete composite. Consequentially, epoxy-coated rebar does not offer an adequate increase in rebar performance in all scenarios, and alternatives are desired.

Stainless Steel Rebar

Stainless steel is an attractive alternative to carbon steel due to its inherently higher corrosion resistance. The term *stainless steel* refers to a class of steels alloyed to improve corrosion resistance, foremost having a chromium content greater than 12% (Nurnberger, 1996). This enables natural formation of a passive, chromium-rich, oxide layer. The corrosion resistance improvements afforded by the chromium addition can be predicted by thermodynamic principles (Pourbaix, 1974). The corrosion resistance can be increased further by the introduction of additional alloying elements such as nickel, molybdenum, or titanium (Sedriks, 1996). The Fe-Cr-Ni alloys are well known to extend the thermodynamic region of passivity to lower pH levels than possible in Fe-C-Mn alloys (Pourbaix, 1974). Moreover, it is expected that Fe-Cr-Ni alloys would

9

possess very high resistances to the pit and crevice corrosion that has been seen under aggregate for carbon steel in concrete (Wilde, 1972). Stainless steel would likely suffer from these forms of localized corrosion at only the most severe chloride concentrations and under only the most oxidizing conditions (Szlarska-Simialowska, 1986). In the event of localized corrosion, attack might propagate more quickly but should be limited to a much smaller area on stainless steel than on carbon steel. Localized corrosion might detrimentally impact the mechanical properties of the rebar, but the effect of oxide formation on concrete performance might be minimal, since corrosion products would be limited to small areas instead of over the entire surface of the rebar. The major drawback to employing stainless steel rebar in construction applications is the increased initial cost over carbon steel. The projected cost for stainless steel rebar is approximately 4 to 8 times greater than the cost of carbon steel rebar, depending on the stainless steel grade (Numberger, 1996). However, the projected lifetime costs of using stainless steel may be lower than those for carbon steel rebar, due to the extended structure lifetimes without the need for costly repair and rehabilitation projects (USDOT, 1998). The degree to which lifetimes are increased and costs are reduced must be more firmly established.

Stainless Steel-Clad Rebar

A stainless steel-cladding over carbon steel is an attractive alternative to solid stainless steel from a cost standpoint. Theoretically, the corrosion resistance of solid stainless steel is obtained at a fraction of the cost. In this study, a type 316L stainless steel-cladding over a carbon steel core was investigated (cladding thickness ≈ 1 mm). Understanding the Cl^- threshold for stainless steel-cladding is the first step towards understanding the degree to which lifetimes may be extended and whether a stainless steel-cladding is equivalent to solid stainless steel of similar composition.

Of great interest is the resulting corrosion behavior when a break in the clad layer, exposing the carbon steel core, is incurred. This exceptional but critical case could be realized through either significant localized corrosion through the clad layer or mechanically induced damage (e.g., construction site handling or even unsealed cut ends) that exposes the carbon steel core. The two situations that expose the carbon steel core are fundamentally different. Pitting corrosion creates an aggressive local environment due to Cr^{+3} hydrolysis and concurrent acidification of the corrosion site. This would result in rapid galvanic corrosion of exposed carbon steel in the acidified pit type environment, should the cladding become penetrated. In the case of a mechanical defect, the localized acidified environment is absent, but the possibility still exists for galvanic corrosion under conditions above the critical chloride threshold associated with corrosion initiation for the underlying carbon steel. Exposure of the carbon steel core by either scenario creates a galvanic couple, with the more noble stainless steel-clad layer being the cathode and carbon steel the anode. The carbon steel core could be anodically polarized from its OCP to a galvanic couple potential between that of passive stainless steel and active carbon steel (Jones, 1996). A detrimental result of the galvanic couple would be an increased rate of corrosion on carbon steel. Galvanic couple behavior is highly dependent on the area of carbon steel core exposed and the area of the stainless steel that can support cathodic reactions (Jones, 1996). Since the total current of the cathode and anode must be equal, large cathode to anode area ratios can significantly increase the anodic corrosion rate at exposed sites. Unfortunately, in the case of a defective stainless steel-clad layer, large cathode to anode area ratios are unavoidable. However, the differences between the OCPs of

carbon steel and clad stainless steel have not been fully explored, and it is unclear whether galvanic corrosion even occurs.

PURPOSE AND SCOPE

In order to justify the increased initial costs of stainless steel or stainless steel-clad rebar, it is necessary to thoroughly investigate their corrosion characteristics. This project was undertaken to investigate some potential benefits and shortcomings regarding the use of a corrosion-resistant rebar substitute in an aggressive concrete environment containing chlorides.

The corrosion characteristics of rebar in concrete can be divided into two stages: an initiation stage and a propagation stage. This project is mainly focused on assessing the extension of the initiation stage afforded by novel rebar materials. Corrosion metrics, such as chloride threshold concentration, do not exist for many new stainless steel candidates. Such information would enable calculation of cost versus lifetime extension. Moreover, it is uncertain whether stainless steel-clad rebar can maintain the same superior corrosion resistance as solid stainless steel rebar, because any exposure of the carbon steel core could result in accelerated corrosion of the anodic carbon steel core due to galvanic coupling to the passive stainless steel-clad layer. Therefore, the effect of cladding defects that expose the carbon steel core on corrosion behavior is a critical consideration. The major concern regarding solid stainless steel is identifying the critical amount of chloride that is necessary to initiate corrosion.

- It must be determined whether the electrochemical corrosion properties of intact clad stainless steel are equivalent to those of solid stainless steel.

- A reliable test method for chloride threshold determination on stainless steels must be selected.

- The chloride threshold concentration for corrosion initiation must be determined for intact and defective stainless steel-clad (exposing the carbon steel core) rebar and compared to that for solid stainless steel. The effect of mechanically produced and corrosion-induced breaks in the stainless steel-cladding on chloride threshold concentrations must be investigated.

- The effect of galvanic coupling between stainless steel and carbon steel on corrosion behavior must be determined both above and below the chloride threshold concentration for corrosion of carbon steel.

- The chloride threshold concentration for corrosion suppression must be determined, since it is a conservative parameter that indicates the conditions where corrosion will not occur.

11

METHODS AND MATERIALS

Materials and Experimental Setup

Types of Reinforcing Bars Investigated

Tests were performed on three types of rebar, AISI A615M carbon steel, 316LN solid stainless steel, and 316L stainless steel-clad over A615M carbon steel. The composition of the rebars is presented in Table 3. The PREN (pitting resistance equivalency number) is a function of Cr, Mo, and N content of the stainless steel and has been used to predict the localized corrosion resistance of stainless steels in Cl⁻ solutions (Sedriks, 1996). The plain steel and solid stainless steel bars were size #5 (diameter ≈ 17.5 mm). The stainless steel-clad bar was size #6 (diameter ≈ 20 mm with the clad layer being 1 to 2 mm thick; see Figure 1.

Table 3. Measured composition of rebars used in study (expressed as wt. %); balance for all bars is Fe. The pitting resistance equivalency number (PREN) is also presented.

Rebar Type	C	P	S	Mn	Si	Cr	Ni	Mo	Cu	Ti	N_2	PREN
AISI 615M Carbon Steel	0.43	0.007	0.038	1.11	0.22	0.03	0.11	<0.01	0.37	--	--	<0.06
Solid SS 316LN	0.026	0.022	0.015	1.486	0.447	17.84	11.775	2.848	0.25	0.006	0.218	30.72
316L Clad Layer	0.044	0.031	0.004	1.33	0.39	16.71	10.16	2.07	0.44	--	.038	24.15

Stainless Steel-Clad Layer

Interface

Rebar Steel Core

1 mm
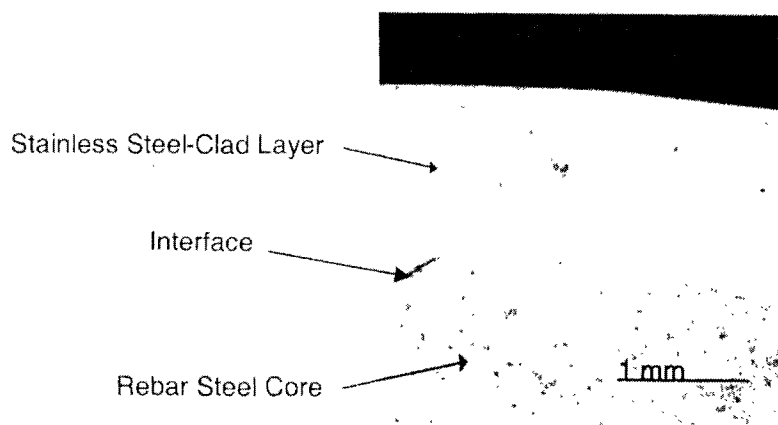
Figure 1. Partial view of the cross-sectional area (transverse section) of 316L stainless steel-clad rebar showing cladding thickness.

12

Electrochemical Cell Design and Use

Electrochemical test methods were used to characterize the corrosion properties of the rebars. Electrochemical methods either accelerate corrosion attack or provide a more sensitive means to detect damage in non-accelerated tests. Electrochemical testing was performed in two types of cells, flat and vertical, which required separate specimen preparations discussed in the following sections. All potentials in this report are versus the saturated calomel electrode (SCE), regardless of the electrode used to make the measurement.

Flat Cell

The flat cell was used for preliminary testing of the polished transverse face of the solid stainless steel or carbon steel rebar, removing any effects of the mill scale. Flat cell experiments used a standard three-electrode electrochemical setup. This configuration was used to determine ranges of Cl^-/OH^- and other parameters to be used in subsequent tests. No results or discussion from these experiments will be presented in this report. More information on the flat cell testing can be found in Hurley (2002).

Vertical Cell

Vertical cell experiments were performed in a custom built three-electrode electrochemical cell, shown schematically in Figure 2. The modified cell design was used to avoid unwanted crevice attack that occurs with specimen/Teflon washer contact on a flat cell and to perform electrochemical testing on the rebar surface that is actually exposed during service. A 1.2-liter acrylic jar was fitted with a Teflon lid and rubber O-ring gasket. The lid contained openings for a reference electrode, a rubber stopper-mounted rebar specimen, and a counter electrode. An SCE with a Luggin capillary probe was used for most experiments. The sensing tip of the Luggin probe
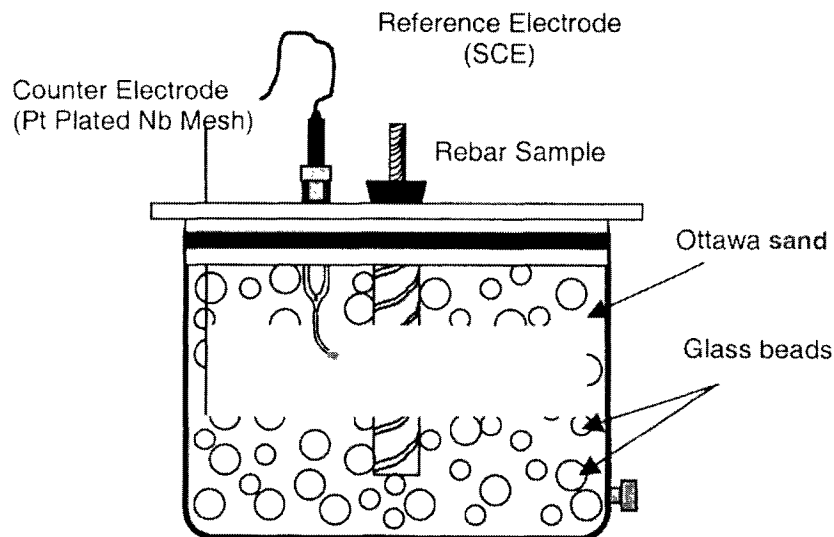
Figure 2. Schematic diagram of the vertical cell configuration used for chloride threshold determination tests in glass bead-sand mixture with saturated $Ca(OH)_2$ plus NaCl solutions.

13

was approximately 10 mm from the sample. For the chloride-free experiments, a Hg/Hg_2SO_4 reference electrode was used, but results were converted to the SCE scale. The cylindrical counter electrode was constructed from platinized niobium mesh, 30.5 cm by 2.5 cm ($\approx$ 152.5 cm^2, although the effective surface area is larger), spot-welded to a platinum-coated titanium rod.

Vertical cell test samples (see Figure 3) were prepared from $\approx$ 70-mm lengths of rebar cut with a DO-ALL band saw. One end of each test piece was drilled, tapped, and fitted with an approximately 40-mm-long piece of 1040 threaded rod. This established electrical contact with the sample and served as a sample holder when threaded into a #3 rubber stopper. Copper paste was added to the interface between the rod and the rebar to enhance electrical contact. The threaded rod was secured to the rebar with a stainless steel hex nut. The threaded rod and nut were masked (MPM Masking 3500) to prevent their contact with the electrolyte and unwanted secondary electrochemical reactions. The working electrode surface area for these specimens was approximately 40 cm^2.
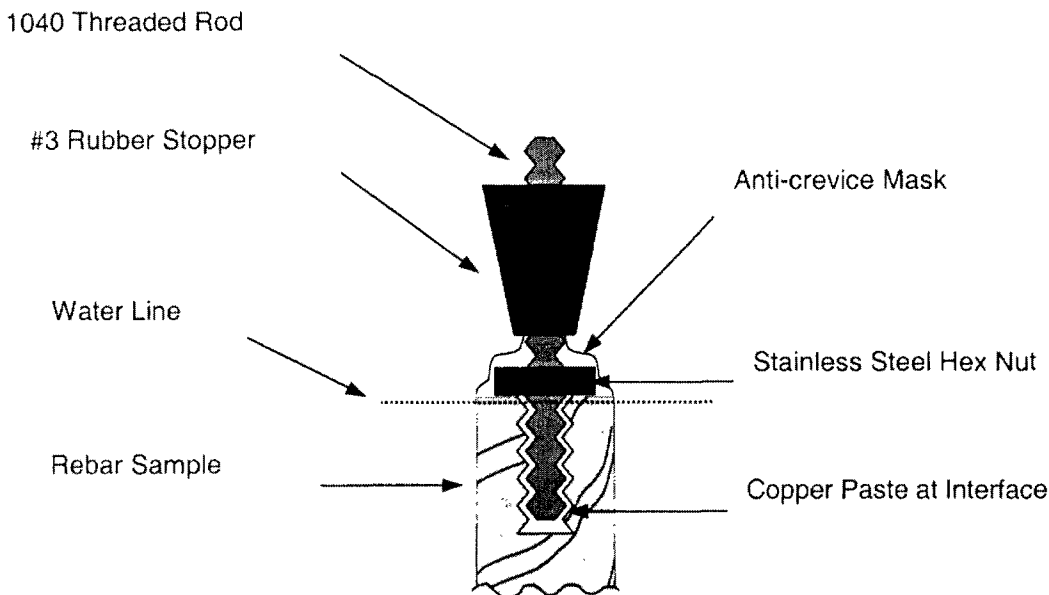
Figure 3. Cross-sectional schematic view of top of rebar sample and electrical connection as prepared for testing in the vertical cell shown in Figure 2.

The as-received carbon steel rebar samples contained a surface covering of black mill scale and small amounts of red rust associated with natural weathering during storage and transportation. In order to minimize test pollution from possible surface contamination incurred during transportation, each rebar specimen was cleaned and then stored in a vacuum desicator until use. The solid stainless steel and the clad stainless steel did not exhibit a voluminous mill scale or the presence of red rust but were still prepared identically to carbon steel for consistency.

The clad stainless steel was tested in a number of configurations:

1. washed, degreased, and ultrasonically cleaned in acetone, rinsed with deionized water, and dried at room temperature

14

2. as in 1, with the exposed end sealed with a 316 weld
3. as in 1, with the exposed end sealed with epoxy (some stainless steel specimens were also prepared this way for comparison)
4. as in 1, with a hole, 3-mm diameter and 3-mm deep (sufficient to expose the carbon steel core), drilled through the cladding and the cut end masked with epoxy
5. as a U-bend specimen to ensure testing on only the intact clad layer with no exposure of the carbon steel core; the U-bend bar contained a 180° bend with a bend radius of ≈ 3.25 cm. The working electrode surface for the U-bend specimens was approximately 65 cm^2

Electrolytes

Two base electrolyte solutions were used in this investigation. Saturated $Ca(OH)_2$ (0.025 M and pH 12.6) and pH 6.2 (adjusted with citric acid monohydrate, $H_3C_6H_5O_7 \cdot H_2O$) solution containing 0.025 M $Ca(OH)_2$. Several chloride levels were produced in each of these solutions by the addition of NaCl (see Table 4). All solutions were prepared with reagent grade chemicals and deionized water (18.2 MΩ-cm resistivity).

For certain tests in the vertical cell, Ottawa sand (ASTM-C109) and glass beads (6-mm and 3-mm diameter) were added. This simulated in-service rebar/concrete-aggregate crevice conditions, high concrete electrical resistivity, and concrete mass transport conditions while also allowing variable chloride levels to be readily selected. This experimental configuration, hereafter referred to as simulated concrete, also enabled rapid examination of test specimen surfaces after testing. Testing in actual concrete makes removing and examining test samples very difficult due to the adhesion and strength of concrete surrounding the rebar. The two sizes of glass beads were used to mimic fine (< 4.75-mm diameter) and course (> 4.75-mm diameter) aggregates. The ratio of 6 mm beads to 3 mm beads was approximately 3:1, and the additional cell volume was filled with Ottawa sand. This configuration gave a theoretical pore volume fraction in agreement with the typical capillary porosity of hydrated cement paste (0.33 for w/c = 0.63 and 100% hydration) (Mehta, 1986).

Table 4. Summary of chloride concentrations used in repassivation studies.

Chloride Concentration (M NaCl added to saturated $Ca(OH)_2$)	$[Cl^-]/[OH^-]$	Hypothetical kg Cl^-/m^3 concrete
0.1	4	1.947
0.01	0.41	.1947
0.008	0.32	.1542
0.003	0.12	.0578
0.001	.042	.01947

15

Experimental Procedures

Chloride-induced corrosion of materials occurs above sharp thresholds in potential, temperature, and chloride concentration. This section defines tests used to determine these parameters. The test procedures were chosen for their applicability to both carbon steel and stainless steel. All tests were conducted at room temperature (23-25 °C) under naturally aerated (un-deaerated) conditions. Not all rebar samples were tested under every set of experimental conditions, since it is unnecessary to test stainless steel at very low (or carbon steel at very high) Cl⁻ /OH⁻ molar ratios. Tests were run two, three, or more times, depending on agreement.

Open Circuit Potential, E_{corr} Determination

Vertical cells with a simulated concrete crevice environment and saturated $Ca(OH)_2$ with 0.1M NaCl ($Cl^-/OH^- = 4$) as well as without chloride were used to test the following rebars: carbon steel; clad stainless steel rebar (defect free) epoxy end-capped; clad stainless steel rebar with a hole drilled through the cladding (3-mm diameter and 3-mm deep); clad stainless steel rebar with end exposed; clad stainless steel U-bend; and solid stainless steel. The two solution environments were used to obtain E_{ocp} data both above (active state) and below (passive state) the literature-reported chloride threshold concentration for plain carbon steel. Additional open circuit experiments were run in saturated $Ca(OH)_2 + 0.1M$ NaCl ($Cl^-/OH^- = 4$) without the simulated concrete for carbon steel, solid stainless steel, and clad stainless steel with a hole drilled through the cladding. The approximate exposed area of carbon steel (for drilled hole and exposed-end clad bar) and subsequent area ratio of stainless steel and carbon steel are presented in Table 5. Two clad rebar defects, drilled hole and exposed end, were used to gain insight into possible potential differences caused by the area of exposed underlying carbon steel. In these cases, a galvanic couple potential was measured. Potentials were measured with a high impedance digital multimeter.

Table 5. Summary of areas associated with defects in stainless steel-clad rebar.

Defect	Exposed Carbon Steel Area (cm²)	Area Ratio of Stainless Steel to Carbon Steel
3-mm diameter by 3-mm deep drilled hole	0.37	108.1
Exposed end	2	20.5

Potentiodynamic Polarization

The general electrochemical corrosion behavior of the rebars as a function of potential was investigated using potentiodynamic polarization scans (E-log(i)). The tests were performed in chloride containing simulated concrete with high pH (12.6) and low pH (6.2) saturated $Ca(OH)_2$ over a range of chloride concentrations. Prior to potentiodynamic polarization scans, samples exposed in laboratory air were allowed to stabilize at their OCP for 1 hour. Scans were performed at a scan rate of 0.167 mV/s. Anodic scans were started at approximately 50 mV below OCP and

continued up to a maximum potential of 1.2 V. Cathodic scans were conducted on the solid stainless steel specimens beginning about 50 mV above OCP and scanning as far down as –1.5 V.

Electrochemical Impedance Spectroscopy, Determination of i_{corr}

EIS was used to determine the polarization resistance (R_p) of the carbon steel, stainless steel, and stainless steel-clad rebar with the drilled hole. EIS experiments were performed in the vertical cell with saturated $Ca(OH)_2$ at pH 12.6 and a chloride concentration of 0.1 M NaCl. Most measurements were taken at open circuit potential, in the frequency range 100 kHz to as low as 1 mHz, with six data points per decade of frequency (scan times were ≈ 30 min). Additional scans of carbon steel were made at –0.3 V, near the galvanic couple potential. The spectra were analyzed with an equivalent circuit (parallel R_p and C in series with R_Ω) model and ZView2 software (see Figure 4), to obtain values of R_p. The polarization resistance was calculated at the low frequency limit with three-point fitting of Nyquist plots. Estimations of the corrosion rates, i_{corr} ($Amps/cm^2$), were made from R_p and a modified Stern-Geary equation (assuming β_a is nearly infinite in the passive region yields Equation 4). β_c was assumed to be 120 mV.

$$i_{corr} = \beta_c / (2.3 \cdot R_p) \qquad (4)$$
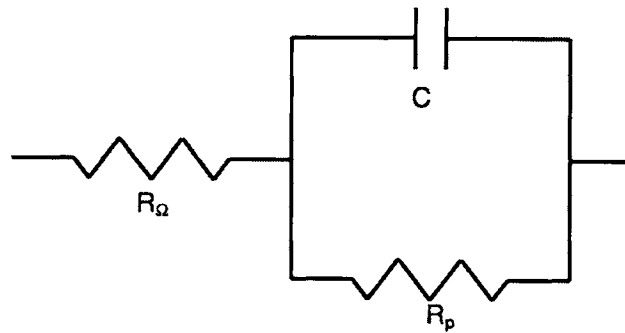
Figure 4. Electrical equivalent circuit model simulating a simple corroding metal/electrolyte interface by parallel connected polarization resistance R_p and capacitance C. R_Ω is the solution resistance. Values of R_p are reported in the units Ω-cm^2 using entire wetted surface area unless otherwise indicated.

Potentiostatic Polarization, Chloride Threshold Determination

The potentiostatic tests were carried out in the vertical cell on carbon steel and solid stainless steel at three potentials: –200 mV, 0 mV, and +200 mV. All tests were carried out in saturated $Ca(OH)_2$ without glass beads/sand to facilitate mixing after each chloride addition. Cl^-/OH^- ratios tested ranged from 0 to saturation (i.e., $Cl^-/OH^- \approx 100$). The first chloride addition was made after a 12 to 24 hour stabilization period, and subsequent chloride additions were made every 12 to 24 hours. This allowed the current sufficient time to stabilize at each chloride level. After a permanent rise in the anodic current density was established above the cutoff current density, 2 to 3 $\mu A/cm^2$, indicative of local corrosion (the actual current density at the local (small

17

active area) corrosion sites will be much greater), the test was terminated. An example is shown in Figure 5. The reported current densities are averaged over the entire electrode area. Maintaining a current density above the cutoff current density ensured steady state active corrosion. Due to the large differences in corrosion resistance among the different rebar materials, a uniform chloride addition for all tests was impractical. To allow similar test durations for all rebars, the chloride increment was customized to each rebar material (see Table 6). The potentiostatic polarization was carried out using either a model 273A EG&G potentiostat or an ESC model 440 multichannel potentiostat. The 273A potentiostat allowed continuous current acquisition (0.01 pts/sec), whereas the 440 required periodic manual measurement of the current.
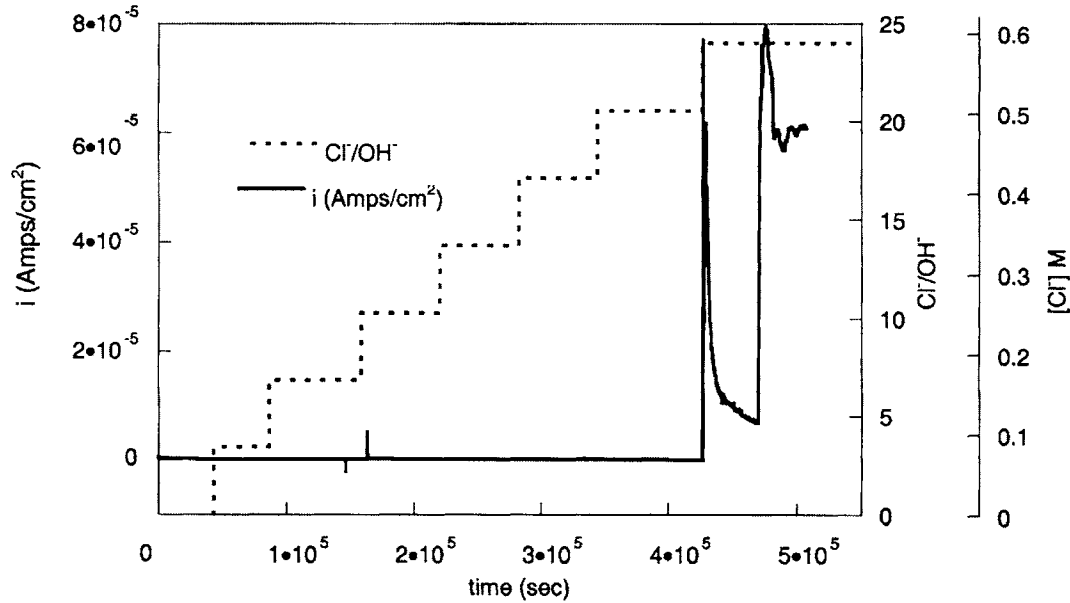
Figure 5. Chloride threshold determination test results on solid 316LN stainless steel rebar showing measured anodic current density versus time (solid line, left axis) as the chloride concentration (dotted line, right axes) is incrementally increased. The chloride concentration is expressed as Cl^-/OH^- molar ratio and chloride molarity. Tests were conducted in saturated $Ca(OH)_2$ + NaCl solution.

Table 6. Chloride addition increments used for chloride threshold determination experiments.

Rebar Material	Chloride Addition Increment	Comments
Carbon Steel	0.15 g	Much lower compared to those of stainless steel
Solid 316LN Stainless Steel	5-20 g	Dependent on potential at which test was conducted
316L Stainless Steel-clad	0.5-5 g	Dependent on condition of the cut end

18

Potential Step Down Determination of E_r

Potential step down experiments were run in the vertical cell to determine E_r. Since the chloride level was constant during each test, simulated concrete was used. The rebar sample was first polarized to 1.5 V for 6000 seconds. This condition is sufficiently aggressive to produce significant local corrosion. The potential was then stepped down to 0.725 V. Each subsequent step down was 75 mV, and the potential was held for 500 seconds to allow stabilization of the crevice current. The step down to 0.725 V was above any foreseeable E_r of an actively corroding sample but low enough not to significantly affect the amount of corrosion damage (the amount of charge collected during the initial step was three orders of magnitude greater than that for each subsequent step). This ensures that no further significant changes to the geometry of the crevice are produced. Therefore, a reliable repassivation potential can be measured minimizing adverse experimental factors such as scan rate dependence.

Each experiment was terminated when the current dropped below 10^{-8} Amps/cm^2 (repassivation of pits and crevices) or became cathodic (potential below open circuit). Experiments were conducted at various chloride concentrations and at pH levels of 12.6 and 6.2. A chloride threshold concentration for corrosion suppression can be found where the E_r abruptly increases with decreasing bulk chloride concentration.

It was important to investigate pit depths less than and greater than the clad layer thickness, exposing the carbon steel core, on the clad rebar. Additional experiments were performed on stainless steel-clad rebar to observe what effect the extent of pitting (crevicing) depth has on the repassivation potential. In an aggressive solution (0.1M NaCl, Cl$^-$/OH$^-$ = 4), the pit propagation times were varied to collect more dissolution charge and increase the severity of corrosion from 5 C/cm^2 to greater than 200 C/cm^2 (sufficient to penetrate the clad layer and expose the carbon steel core).

Mixed Potential Modeling of Galvanic Corrosion

One technique to investigate galvanic couple behavior is to model it using mixed potential theory and experimentally determined potentiodynamic scan data from the known cathode and anode, in this case stainless steel and carbon steel, respectively. The expected galvanic couple potential ($E_{galvanic}$) and corrosion rate (i_{corr}) can be determined from the intersection of appropriately scaled cathodic and anodic curves as shown in Figure 6.
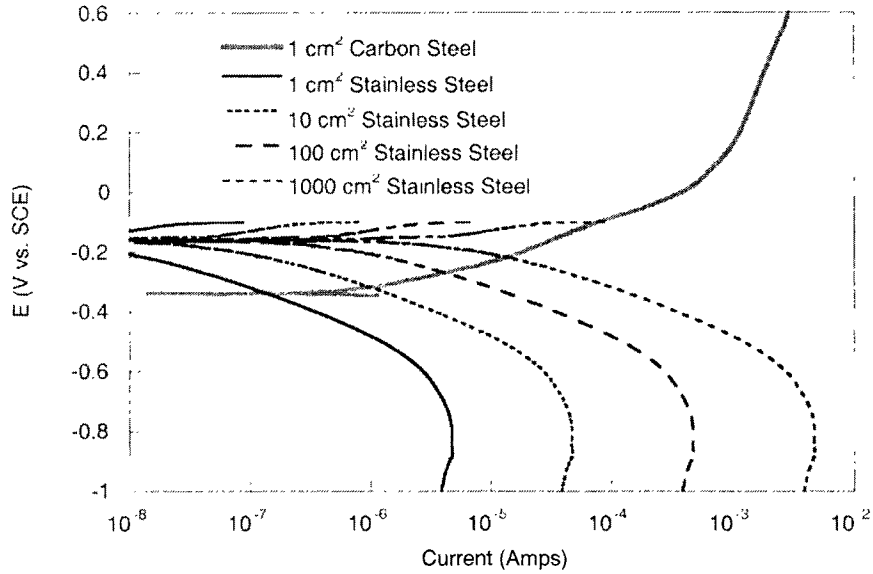
Figure 6. Galvanic couple potentials and currents predicted by overlaying cathodic curves from solid 316LN stainless steel rebar (black) with an anodic curve from an active carbon steel rebar (gray) specimen in saturated $Ca(OH)_2$ solution + 0.1 M NaCl ($Cl^-/OH^- = 4$).

Ohmic resistance lowers galvanic corrosion rates so its effect on active or passive carbon steel cores coupled to passive stainless steel-cladding was estimated for a range of cathode/anode area ratios. Calculations were made to estimate the length of rebar, and hence resistive path length in concrete, needed to satisfy cathode/anode area ratios of 1/1, 10/1, 100/1, and 1000/1 for different defect sizes (0.1 cm^2, 0.37 cm^2 [similar to clad bar with a drilled hole], and 1 cm^2). The ohmic resistance associated with concrete can be estimated from the following relationship (Macdonald et al., 1998):

$$R_{concrete} = \rho_{concrete} \cdot L / A \qquad (5)$$

$R_{concrete}$ is the resistance in ohms, $\rho_{concrete}$ is the concrete resistivity (in ohm-cm), L is the length in cm and A is the cross sectional area in cm^2. It was assumed that rebars are spaced 20 cm apart in concrete and the resulting electrical activity is restricted to a cylindrical volume with a radius of 10 cm, whose long axis is the same as the rebar (Macdonald et al., 1998). The $\rho_{concrete}$ was calculated for the simulated concrete environment with saturated $Ca(OH)_2$ + 0.1 M NaCl. The maximum ohmic voltage between physically separated anodes and cathodes was calculated with the following formula:

$$V_\Omega = I_{galvanic} \cdot R_{concrete} \qquad (6)$$

where V_Ω is in Volts, $I_{galvanic}$ is the galvanic corrosion current in Amps, and $R_{concrete}$ is the resistance associated with concrete for the given cathode area (bar length) in ohms. Anode /cathode area ratios resulting in V_Ω greater than several mV were not considered.

20

Galvanic corrosion predictions for a mechanically created defect in the cladding (exposing the core) were constructed directly from anodic carbon steel and cathodic stainless steel potentiodynamic scans. For an electrochemically induced break in the cladding caused by pitting with the aggressive, low pH environment caused by metal ion hydrolysis, the anodic kinetics for pit dissolution were extracted from the potential step down data

Ohmic Correction of E-log(i) Data

The E-log(i) plots constructed for the mixed potential models were corrected for their own ohmic resistance error due to specimen geometry and solution resistance. The desire was to produce true E-i kinetics on the carbon steel core by calculating the true potential (E_{true}) from the measured potential. Details of the ohmic correction can be found in Hurley (2002).

RESULTS

Carbon Steel Rebar

Potentiodynamic polarization (E-log(i)) tests (plots not shown) indicated that plain carbon steel rebar is passive at OCP in the chloride-free simulated concrete environment at a pH of 12.6 with an $i_{corr} \approx 0.98 \ \mu A/cm^2$. Inspection of E-log(i) curve demonstrated that the carbon steel was passive over a broad range in potentials. The i_{corr} value is slightly high given the short-term nature of the test but is properly normalized to the entire electrode area. Note that literature reports of moderate corrosion rates at 0.5 to 1.0 $\mu A/cm^2$ are erroneous due to uncertainty over actively corroding areas. For instance, if 1 to 10% of the area is actively corroding, then the actual corrosion rates range from 5 to 10 or 50 to 1000 $\mu A/cm^2$. These rates are much more reasonable for actively corroding steel. Oxygen evolution due to the oxidation of water is reached (≈ 0.6 V) prior to achieving any pitting potentials associated with Cl⁻-induced pitting. Plain carbon steel corrodes actively between chloride concentrations of 0.01 M and 0.1 M (Cl⁻/OH⁻ molar ratios between 0.41 and 4). This change to active corrosion results in a lower OCP, –500 mV compared to –100 mV, and higher corrosion current density when normalized over the entire area, 1.8 $\mu A/cm^2$ versus 0.98 $\mu A/cm^2$. Carbon steel rebar becomes active in solutions containing between 0.001 and 0.01 M Cl⁻ (Cl⁻/OH⁻ molar ratios between 0.041 and 0.41) at a pH of 6.2.

The long-term OCP of carbon steel is much lower in 0.1 M NaCl (Cl⁻/OH⁻ = 4) solution compared to the chloride-free solution (–550 mV vs. –100 mV) due to corrosion initiation, as seen in Figure 7. However, the OCP is equal to or greater than that of stainless steel when passive in saturated Ca(OH)₂ solution without Cl⁻ (Figure 7). Thus, OCP tests also indicated corrosion initiation in the case of carbon steel. Corrosion products formed over a large fraction of the rebar in the chloride solution also indicated depassivation over a large surface area, as shown in Figure 8.
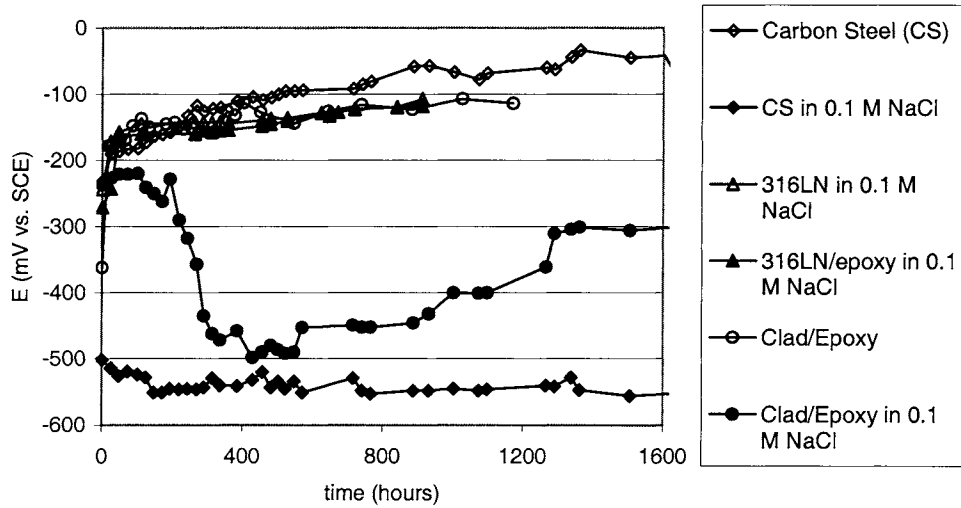
Figure 7. OCP Results for plain carbon steel (CS), solid 316LN stainless steel (316LN), and 316L-clad stainless steel (clad) rebar specimens with and without chloride additions. Testing was conducted in sand-glass beads with saturated $Ca(OH)_2$ solution. Tests containing saturated $Ca(OH)_2 + 0.1$ M NaCl (Cl^-/OH^- = 4) are indicated in the legend.

Carbon steel rebar exhibits a low R_p, indicating an active surface in the chloride containing saturated $Ca(OH)_2$ above its chloride threshold (0.1 M NaCl, Cl^-/OH^- = 4). EIS determination of the polarization resistance ($R_p \approx 50$ $k\Omega$-cm^2) indicates an i_{corr} of 1.3 $\mu A/cm^2$ when normalized over the entire working electrode area. If active corrosion is localized, the current density would be greater at each site.
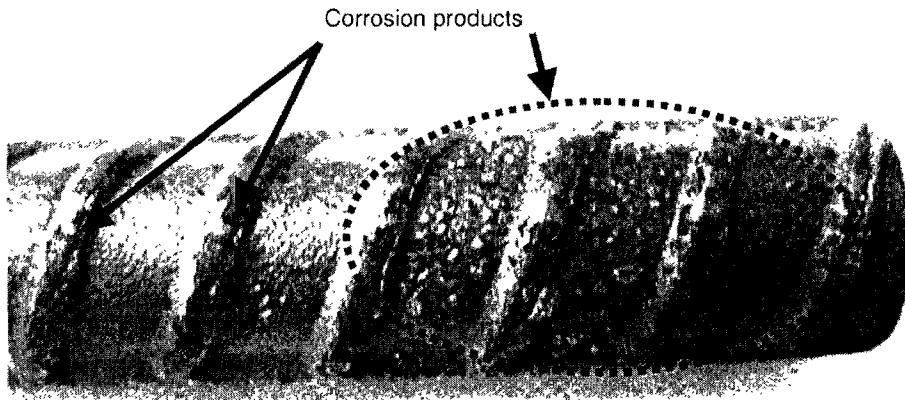
Figure 8. Carbon steel rebar sample after open circuit potential testing; sample was tested in simulated concrete with 0.1 M NaCl added (Cl^-/OH^- = 4). Formation of corrosion products over a large fraction of the surface indicates general as opposed to localized depassivation.

22

The chloride threshold concentration for corrosion initiation determined from potentiostatic tests on carbon steel was very low at all potentials tested (initiation occurred at Cl^-/OH^- molar ratio ≤ 1.5), as shown in Figure 9. This result is in agreement with values reported in the literature (see Table 1).
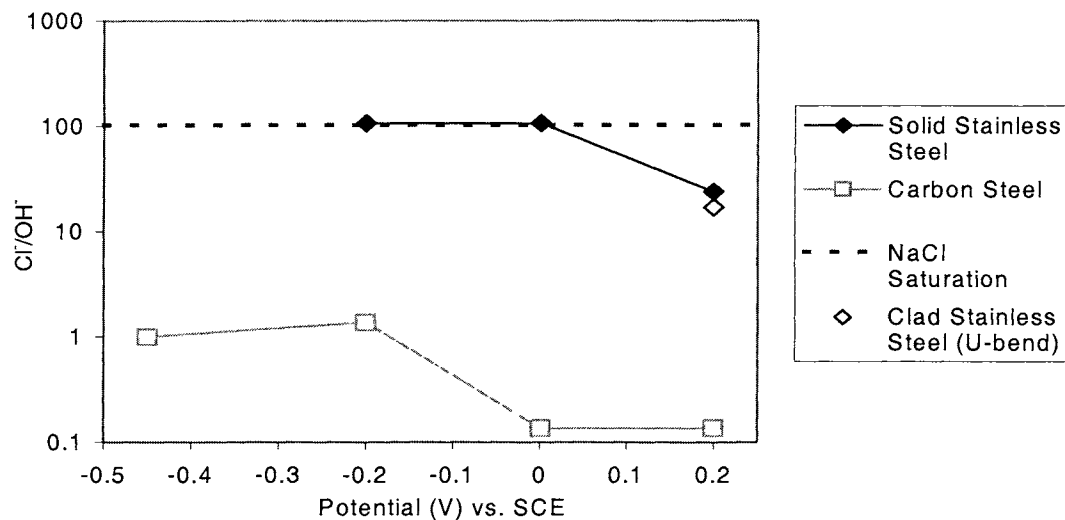

Figure 9. **Chloride threshold concentration as function of applied potential for corrosion initiation of plain carbon steel and stainless steel rebars in saturated Ca(OH)₂. Test results at 0.0 and -0.2 V (vs. SCE) did not initiate corrosion in the case of solid 316LN stainless steel. The value presented for 316L clad rebar represents a best value, acquired from a U-bend specimen test.**

The step down repassivation potential results are shown in Figure 10. These results are more conservative than those obtained from potential scans, as shown by comparison in Figure 11. In the case of plain carbon steel, the current becomes cathodic at "E_r", instead of repassivating by reformation of a protective oxide film, as the potential is decreased. Active corrosion on carbon steel, once initiated, can still be sustained at a chloride concentration as low as 0.001M NaCl ($Cl^-/OH^- = 0.041$). Therefore, the chloride threshold for corrosion suppression on carbon steel is some value less than 0.001M NaCl ($Cl^-/OH^- = 0.041$) in short-term lab tests. Post-test visual examination shows large pits that have coalesced or widened into craters occupying a large fraction of the surface area on carbon steel (see Figure 12).
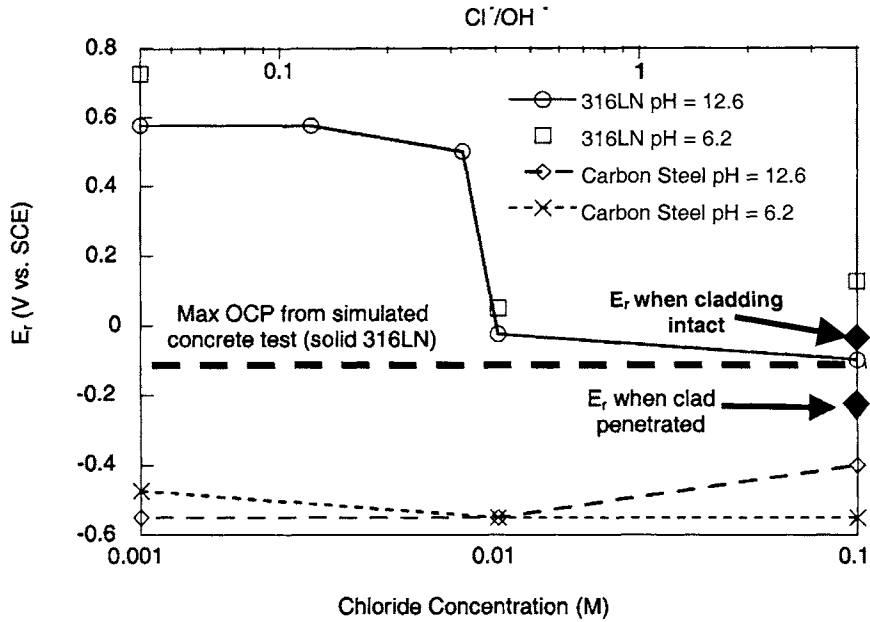
Figure 10. Repassivation potentials for solid 316LN and plain carbon steel versus chloride concentration. Testing was conducted in sand-glass beads with saturated Ca(OH)₂ + NaCl solution at pH 12.6 and 6.2 (buffered with citric acid). E_r for intact clad rebar was similar to the solid 316LN rebar.
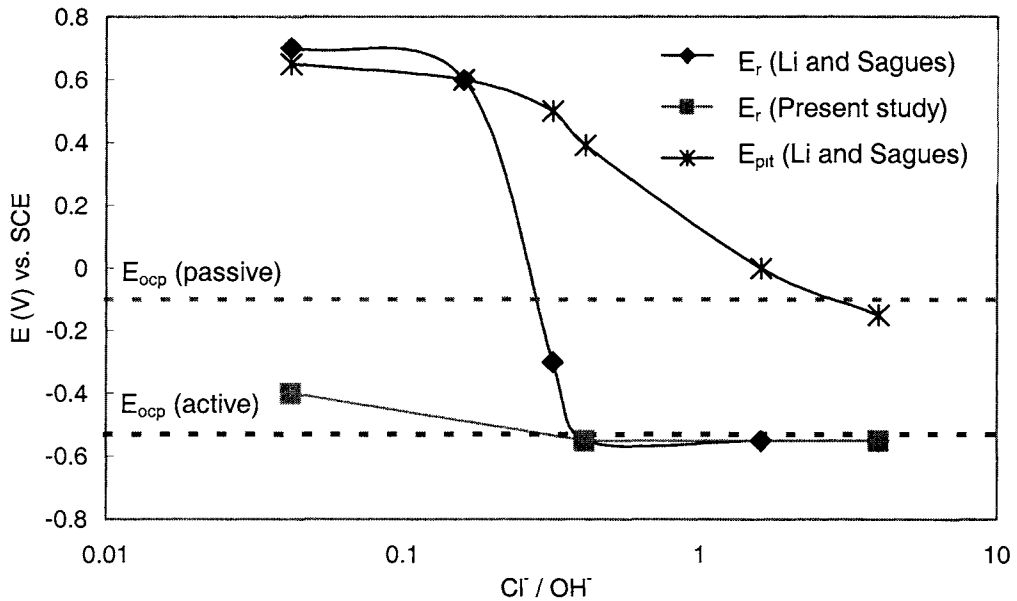

Figure 11. Repassivation (E_r) and pitting potential (E_pit) values obtained for plain carbon steel from different experimental techniques versus chloride concentration, conducted in saturated Ca(OH)₂ + NaCl solution. Also shown are OCP values for carbon steel above (active) and below (passive) the chloride threshold for corrosion initiation. E_r and E_pit from Li (Li and Sagues, 1999) were obtained from potentiodynamic scans. E_r (square symbol this study) was obtained from the step down method in this study.

Figure 12. Visual appearance of carbon steel rebar repassivation specimen after potential step down test, conducted in sand-glass beads with saturated Ca(OH)$_2$ + 0.1 M NaCl solution (Cl$^-$/OH$^-$ = 4).

Solid 316LN Stainless Steel Rebar

Solid 316LN stainless steel rebar remained passive at all chloride levels tested by potentiodynamic polarization (E-log(i)) at a pH of 12.6 (E-log(i) curves not shown). Oxygen evolution due to the oxidation of water occurs ($\approx$ 0.6 V) prior to reaching a pitting potential associated with Cl$^-$-induced pitting. Hence, E_{pit} from a potential scan cannot be used to determine chloride initiation thresholds (Figure 13). The rebar also remained passive at 0.01 M NaCl (Cl$^-$/OH$^-$ = 4) and pH = 6.2, although metastable pitting was observed above 0.4 V (E-log(i) curves not shown). The i_{corr} estimated from E-log(i) data increased from 0.03 μA/cm^2 seen at 0.1 M NaCl (Cl$^-$/OH$^-$ = 4) and pH = 12.6 to 0.55 μA/cm^2 at 0.01 M NaCl (Cl$^-$/OH$^-$ = 0.4) and pH = 6.2. These data were normalized to total surface area, which was reasonable since pitting was not observed.
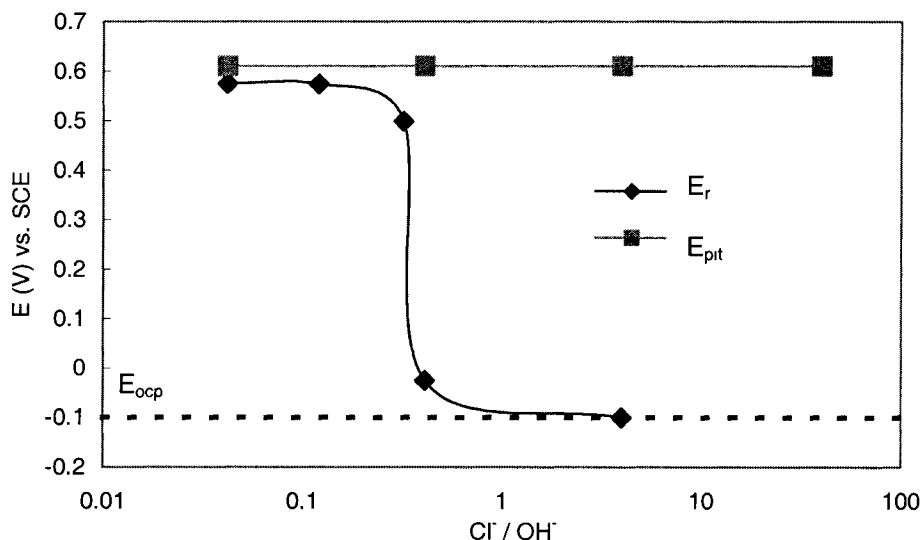

Figure 13. Pitting potentials (E_{pit}) from potentiodynamic scans compared to repassivation values (E_r) obtained from potential step down tests following corrosion initiation on solid 316LN. The values of E_{pit} indicated represent oxygen evolution and do not represent pitting. Hence meaningful E_{pit} and E_r values could not be obtained from potentiodynamic scans in the case of 316LN.

25

The long-term OCP results are shown in Figure 7. All OCP values for solid 316LN stainless steel were approximately –150 to –50 mV. The OCP values rise over time, suggesting that chloride thresholds must be determined over a range of potentials. Open circuit potentials for solid stainless steel exhibit no effect of chloride even at the highest concentrations tested (0.1 M NaCl, $Cl^-/OH^- = 4$). No meaningful difference was detected between samples tested with and without epoxy sealing over the cut end of solid 316LN stainless steel. Post-test visual inspection did not reveal any sign of corrosion or crevicing due to the simulated concrete or the epoxy.

EIS determination of the polarization resistance of 316LN stainless steel yielded a value of 10 MΩ-cm^2 in the 0.1 M NaCl ($Cl^-/OH^- = 4$). This indicates a corrosion rate, i_{corr}, of 0.18 μA/cm^2 when normalized to the entire specimen area. The 316LN exhibits a very high polarization resistance, indicative of passivity.

The chloride threshold for initiation of stable active corrosion of solid stainless steel rebar polarized at +200 mV occurs at a Cl^-/OH^- molar ratio of 24, as shown in Figure 9. This is consistent with values in the literature (see Table 2). Solid 316LN stainless steel polarized to –200 mV and 0 mV did not show passivity breakdown or corrosion initiation, even at a Cl^-/OH^- molar ratio of 100. The threshold could not be determined for these potentials in 24 h potentiostatic tests because the rebar was still passive when the solutions became saturated with NaCl ($Cl^-/OH^- \approx 100$).

The repassivation potential results for solid 316LN stainless steel are shown in Figures 10 and 13. It can be seen in Figure 13 that apparent critical threshold potentials (E_{pit}) determined by potentiodynamic scanning methods do not indicate Cl^- induced corrosion initiation. Instead, apparent E_{pit} values indicate oxygen evolution. A significant drop in repassivation potential (from +0.5 to –0.025 V) is seen between 0.008 M ($Cl^-/OH^- = 0.32$) and 0.01 M NaCl ($Cl^-/OH^- = 0.41$), with little effect of pH (Figure 10). Thus, the chloride threshold below which any local corrosion, if ever initiated, would be suppressed occurs over the same range of Cl^-/OH^- molar ratios. E_r appears to be roughly independent of the amount of corrosion damage on solid stainless steel as shown in Figure 14. Visual inspection shows distinct, high aspect ratio pits on the stainless steel after tests where pits were initiated and then repassivated, while the remainder of the specimen remained passive (see Figure 15).
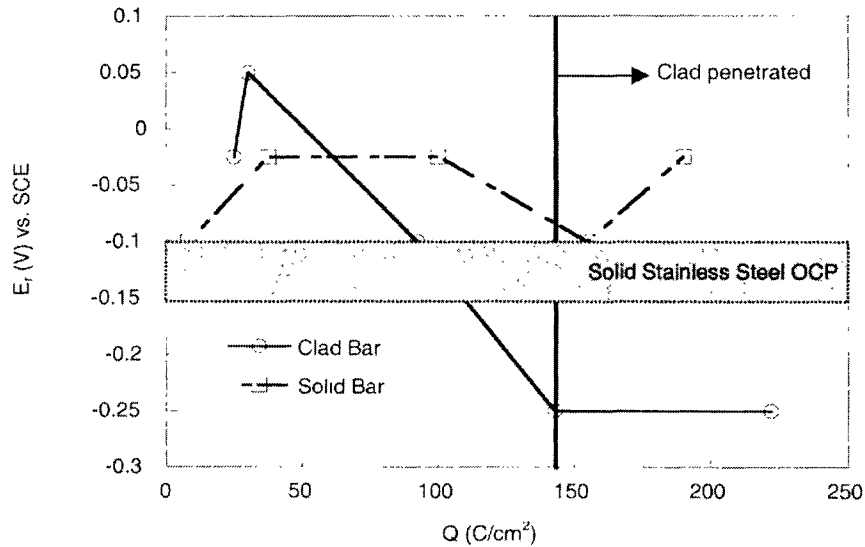
26

Figure 14. Repassivation potential (E_r) as a function of corrosion damage, expressed as anodic charge density, for solid 316LN stainless steel and 316L stainless steel clad. Tests conducted in sand-glass beads with saturated $Ca(OH)_2$ + 0.1 M NaCl solution (Cl^-/OH^- = 4). The OCP range of stainless steels is indicated. The vertical line indicates the charge density above which cladding penetration was observed.

Figure 15. Post-test appearance of solid 316LN stainless steel rebar repassivation specimen. Test was conducted in sand-glass beads with saturated $Ca(OH)_2$ + 0.1 M NaCl solution (Cl^-/OH^- = 4).

316L Stainless Steel-Clad Rebar

Intact Clad Rebar

Weld-Sealed-End Clad Rebar Specimens

The initial chloride threshold test on intact 316L-clad rebar, with 316 stainless steel welded over the cut end, resulted in significant corrosion products, including red rust, formed preferentially

27

at the weld (Figure 16). A low threshold Cl⁻ concentration was observed ($Cl^-/OH^- = 3.4$), as reported in Figure 17. This welded type specimen was not investigated further.
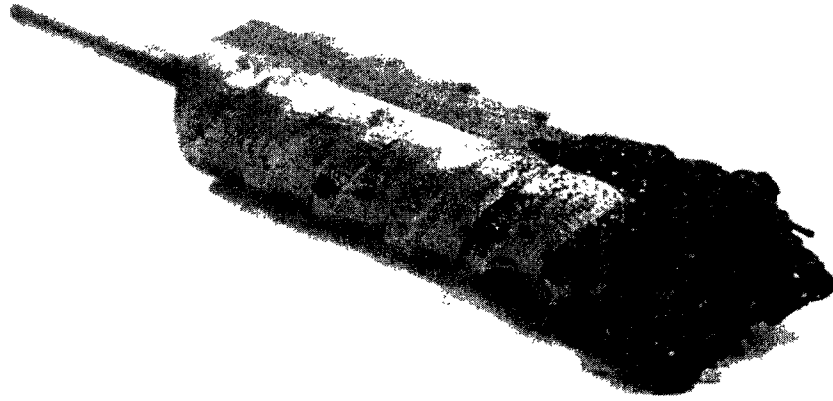

Figure 16. Appearance of 316L stainless steel-clad rebar with the cut end sealed by welding with 316 to cover the exposed carbon steel core, after chloride threshold testing at +200 mV (vs. SCE). Tests were conducted in saturated $Ca(OH)_2$ + NaCl solution.
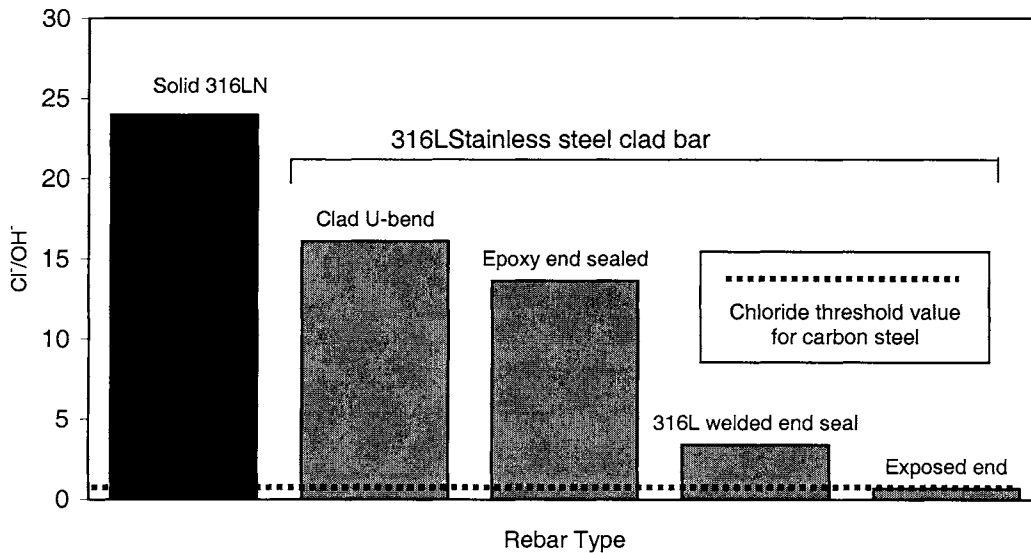

Figure 17. Chloride threshold concentration values at +200 mV, expressed as Cl^-/OH^- molar ratio, for several preparations of the 316L stainless steel clad rebar. Results indicated for U-bend and epoxy-sealed end are averages. The high value for both the U-bend and epoxy-end-sealed specimens was $Cl^-/OH^- = 17$. Results for solid 316LN and carbon steel are also shown for comparison.

28

Epoxy-Sealed-End Clad Rebar Specimens

The OCP results for the epoxy-sealed 316L-clad rebar are similar to those for solid stainless steel, approximately −150 mV (carbon steel was −100 mV), in the chloride-free environment (0 M NaCl, $Cl^-/OH^- = 0$), as shown in Figure 7. This indicates similar passive corrosion rates on well-sealed 316L-cladding as seen for solid 316LN stainless steel. However, post-test visual inspection of the specimen tested in 0.1 M NaCl ($Cl^-/OH^- = 4$) revealed some corrosion around the epoxy.

The chloride threshold at +200 mV varied from $Cl^-/OH^- = 10$ (0.25 M NaCl) to $Cl^-/OH^- = 17$ (0.43 M NaCl) with an average value of 13.5 (two samples) reported in Figure 17. Corrosion products were observed beneath the epoxy of both specimens, indicating that some plain carbon steel may have been exposed to the environment, providing the site for easier chloride-induced corrosion.

The repassivation potential results for clad stainless steel are shown in Figures 10 and 14. At a low anodic charge (Q) indicative of small pits (anodic charge can be related to corrosion depth; these tests were conducted at depths less than the clad thickness), E_r is roughly independent of the amount of pitting damage and similar to that for solid 316LN stainless steel before the cladding is penetrated. However, once the cladding is breached, exposing the underlying plain carbon steel (see Figures 14 and 18), E_r drops dramatically.
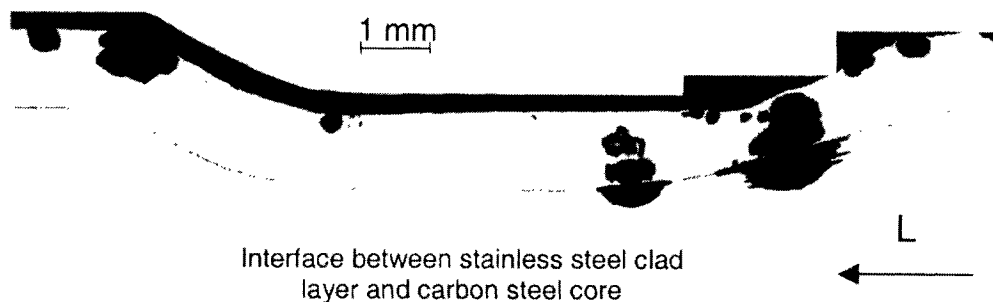

Figure 18. Composite optical micrograph of a longitudinal cross section of 316L stainless steel-clad rebar after repassivation potential testing in saturated $Ca(OH)_2$ + NaCl solution. When pits penetrate the clad layer (top), rapid attack occurs at the clad/core interface in the underlying carbon steel (bottom). The interface between the cladding (above) and core (below) has been enhanced with a gray line.

U-Bend Clad Rebar Specimens

The OCP results for the U-bend 316L-clad rebar are shown in Figure 19. OCP values are nearly identical with those of 316LN solid stainless steel (approximately −150 mV) and slightly (50 mV) less than for passive carbon steel (Figure 7). This, again, indicates similar passive corrosion rates as seen for solid 316LN stainless steel.
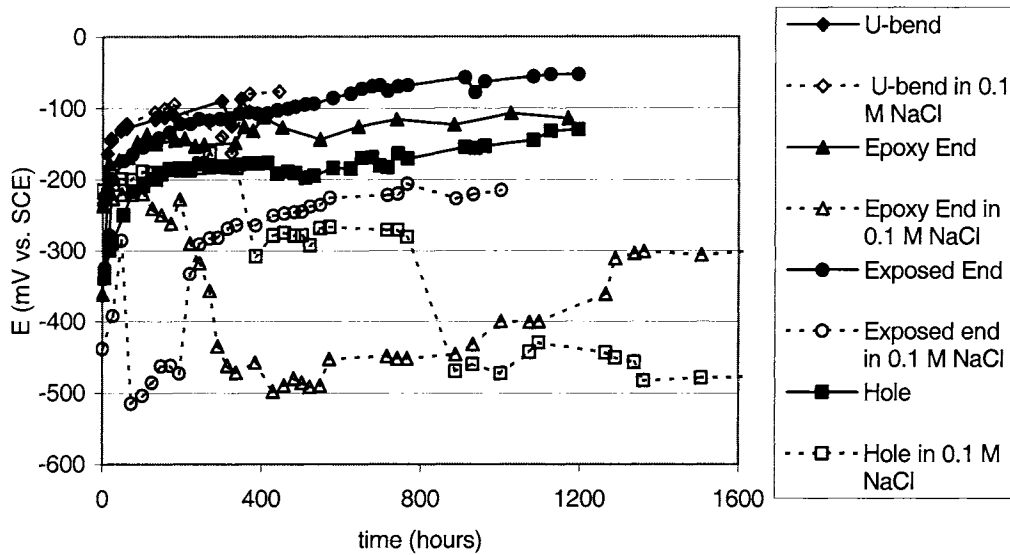
Figure 19. OCP results for the 316L-clad rebar samples in sand glass beads with saturated Ca(OH)$_2$ + 0.1 M NaCl solution (Cl$^-$/OH$^-$ = 4) (dashed line/open symbol) and in saturated Ca(OH)$_2$ without chloride additions (solid line/solid symbol).

The chloride threshold at +200 mV ranged from Cl$^-$/OH$^-$ = 15 to Cl$^-$/OH$^-$ = 17 ([NaCl] = 0.4 M). An average value of 16 is reported in Figure 17. Corrosion products were observed beneath a skin that formed at the water line. The skin could be a result of CaCO$_3$ formation or evaporation of water, resulting in Ca(OH)$_2$ saturation and salt deposition.

Intentional Mechanical Defect in Cladding

Drilled Hole and Epoxy-Sealed-End Clad Rebar Specimens

The OCP for the 316L-clad rebar with a drilled hole, conducted in saturated Ca(OH)$_2$ with 0.1 M NaCl (Cl$^-$/OH$^-$ = 4), is shown in Figure 19. A potential drop, indicative of active corrosion, is observed for specimens where the Cl$^-$/OH$^-$ exceeds the chloride threshold for corrosion initiation of the exposed carbon steel. This is observed for each case where carbon steel was exposed, whether a drilled hole, cut end, or poor epoxy-sealed end was tested. A potential drop was not observed for the U-bend specimen that does not expose carbon steel (Figure 19). Post-test visual inspection revealed some corrosion around the hole (see Figure 20). The OCP of the clad specimen with a hole in saturated Ca(OH)$_2$ + 0.1 M NaCl is initially at −200 mV, but then drops to about −300 mV and as low as −500 mV. These potentials are between those for solid 316LN stainless steel and active carbon steel, suggesting a mixed potential due to galvanic coupling.
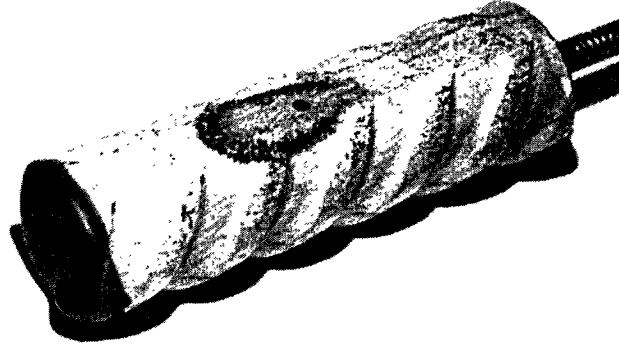
30

Figure 20. 316L stainless steel-clad rebar with cut end sealed with epoxy and a hole drilled to expose the plain carbon steel core. Corrosion products were observed around the drilled hole. Results are from OCP test conducted in sand-glass beads with saturated $Ca(OH)_2$ + 0.1 M NaCl solution (Cl^-/OH^- = 4).

Clad Rebar Specimens with Exposed End

The OCP for the clad rebar with the cut end uncovered (exposing the carbon steel core) is also shown in Figure 19. For the test conducted in saturated $Ca(OH)_2$ solution with no NaCl, the OCP is nearly identical to that of passive carbon steel in a chloride-free environment, approximately –100 mV. In 0.1 M NaCl (Cl^-/OH^- = 4), the corrosion potential initially indicates active corrosion (–500 mV) but elevates to a potential between that of active carbon steel and passive stainless steel ($\approx$ –250 mV). This elevated potential is likely due to galvanic coupling between the passive clad layer and the active carbon steel core. The corrosion damage was limited to the carbon steel core (see Figure 21).

The chloride threshold at +200mV for this sample was similar to that for carbon steel (Cl^-/OH^- = 0.68), see Figure 17.

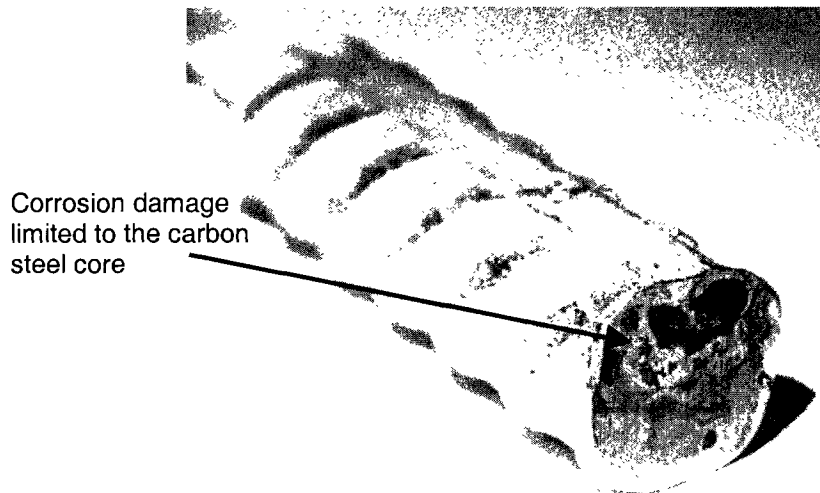Corrosion damage limited to the carbon steel core

Figure 21. 316L stainless steel-clad rebar specimen with a cut end exposed after OCP testing. Corrosion products were seen only on the carbon steel core after testing in sand-glass beads with $Ca(OH)_2$ + 0.1 M NaCl solution (Cl^-/OH^- = 4).

Galvanically Coupled Stainless and Carbon Steel

Prediction of Galvanic Corrosion Rates After Mechanical Damage of Cladding

Figure 22 shows the effect of the cathode/anode ratio on galvanic couple potential, E_{couple}, and the galvanic corrosion rate, i_{corr}, established from mixed potential theory with ohmic voltages. The galvanic couple potential associated with the passive carbon steel obtained from anodic E-log(i)
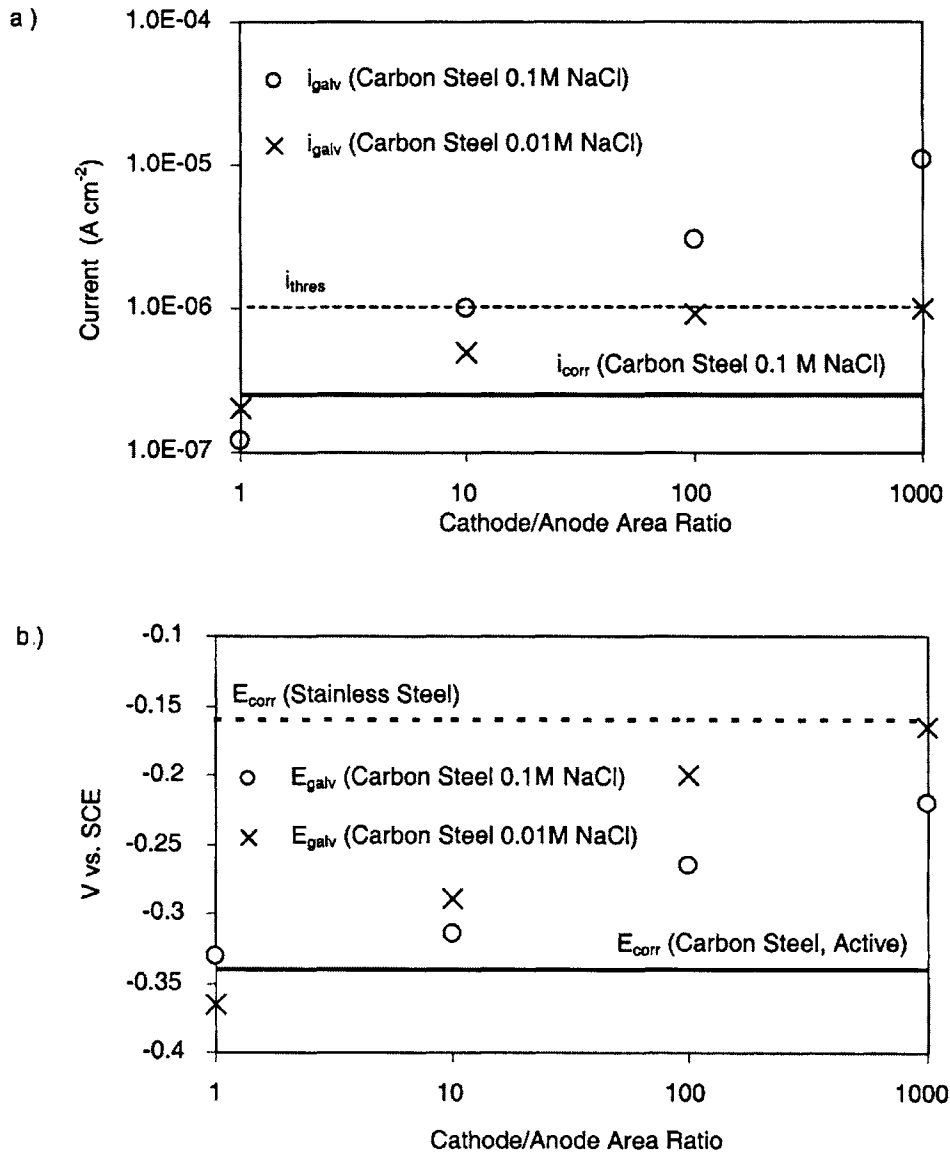
Figure 22. Galvanic current (a) and potential (b) predicted from mixed potential theory for a 1 cm^2 carbon steel coupled to solid 316LN stainless steel at the area ratios indicated exposed in saturated Ca(OH)$_2$ at Cl$^-$/OH$^-$ of 4 (0.1 M NaCl) and 0.4 (0.01 M NaCl). i_{thres} indicates the threshold corrosion rate for active carbon steel according to (Bentour, 1997). E_{corr} indicates the predicted galvanic couple potentials.

scan (0.01 M NaCl, $Cl^-/OH^- = 0.41$) rises sharply with increasing cathode area. As the cathode/anode area ratio is increased from 1 to 1000, the galvanic couple potential rises approximately 200 mV. However, increases in the couple potential result in little or no increase in the corrosion rate (0.3 $\mu A/cm^2$) of the passive carbon steel. A slow increase in corrosion rate is observed initially toward 1 $\mu A/cm^2$, but it remains constant as the cathode to anode area ratio is increased from 100 to 1000.

For the couple of stainless steel to active carbon steel (exposed above its chloride threshold, in 0.1 M NaCl, $Cl^-/OH^- = 4$), the corrosion rate, i_{corr}, increases by almost 2 orders of magnitude, from 0.2 to 10 $\mu A/cm^2$, as the cathode (stainless steel) to anode (carbon steel) area ratio is increased from 1 to 1000. E_{couple} rises more slowly than in the passive case and remains between that of active carbon steel and passive 316L stainless steel. The carbon steel core of 316L stainless steel-clad rebar would exhibit a much faster dissolution rate with decreasing hole size because of the more unfavorable cathode/anode area ratio.

Possible lowering of i_{corr} due to concrete resistance between separated anodes and cathodes was found to be significant at only the largest defect size (1 cm^2) with the largest cathode/anode ratio (1000/1). Even under these extreme conditions, the voltage drop is less than 2 mV. Therefore, the increases in corrosion rate reported for large cathode/anode area ratios predicted from mixed potential theory without consideration of ohmic voltages are reasonable.

Prediction of Galvanic Corrosion Rates After Corrosion-Induced Penetration of Cladding

Additional experiments explored the effect of cathode/anode ratio on E_{couple} and i_{corr} in an environment produced by corrosion-induced penetration of the stainless steel-cladding, which produces an acidified environment. The predicted galvanic corrosion current for corrosion-induced galvanic coupling is approximately an order of magnitude more severe than that for mechanically induced galvanic coupling (curves not shown). This result was obtained for all cathode/anode area ratios.

DISCUSSION

There are two primary issues in this study. The first issue is the performance of solid or intact stainless steel-clad rebar compared to plain carbon steel, and the second is a comparison of stainless steel-clad rebar to solid stainless steel. The 316L (clad) and 316LN (solid) type stainless steels were expected to have a higher intrinsic corrosion resistance than plain carbon steel rebar from knowledge of empirically derived relationships for resistance to Cl^--induced corrosion, such as the PREN. Moreover, threshold potentials and chloride concentrations for corrosion initiation were expected to be greater. This was, indeed, observed. The following discussion is intended to help clarify some of the complexities associated with the data and provides added interpretation of data that contributes to the achievement of the project goals.

Interpretation of Open Circuit Potential Trends

Plain carbon steel, 316L, and 316LN stainless steels are all passive in chloride-free concrete at pH values above 11.5. This results in OCPs for plain carbon steel that start at fairly positive values and rise over time, as indicated in Figure 7. The OCPs of intact clad and solid stainless steel also rise with time (Figures 7 and 19). The low anodic reaction rate associated with the passive state is the cause of a positive OCP value. The slightly higher OCP of plain carbon steel compared to that of 316L or 316LN stainless steel in chloride-free simulated concrete is likely due to a faster cathodic reaction rate on the carbon steel, since chromium inhibits the oxygen reduction reaction. For rebar in concrete exposed to atmospheric conditions, the free corrosion potential typically ranges between -150 to $+50$ mV (Bertolini et al., 1996). OCP results obtained in this study are in agreement, ranging from -250 mV to -40 mV. An increase in thickness of the protective passive film over time accounts for the potential rise. If the potential rise indicated in Figures 7 and 19 continued with additional exposure time beyond the test period, OCPs as high as $+200$ mV might be reached. Therefore, the value of $+200$ mV is viewed as a conservative upper limit for the open circuit potentials of passive plain carbon steel and stainless steel rebars in concrete. These results point to the need for and justifies testing for Cl⁻ threshold concentrations over a range of applied potentials as high as $+200$ mV to obtain Cl⁻ thresholds at upper bound potentials.

When the chloride concentration is increased, the pitting potential (E_{pit}) becomes depressed (Sedriks, 1996). An OCP above the E_{pit} cannot be achieved for very long under these circumstances since the anodic reaction becomes non-polarizable under this condition. Therefore, the decrease in E_{pit} eventually leads to a drop in the OCP with time and an increased corrosion rate. This explains the OCP drop exhibited for plain carbon steel and defective stainless steel-clad rebar under conditions that exposed the carbon steel core to a high Cl⁻ concentration, as seen in Figures 7 and 19. This drop occurred for carbon steel or clad stainless steel with the carbon steel core exposed only when the Cl⁻ concentration was above the Cl⁻ threshold concentration for corrosion initiation of carbon steel. In no cases did the potential drop occur for solid or U-bend clad stainless steel. This indicates two things. The first is that solid stainless steel is unlikely to initiate corrosion at its OCP after long times even if the Cl⁻/OH⁻ molar ratio is 4. It also indicates that intact stainless steel-cladding enjoys a similar resistance against Cl⁻-induced pitting as seen for solid 316LN rebar at Cl⁻/OH⁻ molar ratios of 4. The main difference in OCP between solid 316LN stainless steel and 316L-clad stainless steel with epoxy-coated ends is likely due to ineffective sealing and exposure of the carbon steel core. The chloride threshold for the carbon steel core is exceeded in the case of a 316L-clad rebar with the drilled hole when exposed in an 0.1 M NaCl (Cl⁻/OH⁻ = 4) simulated concrete solution. Thus, the OCP also decreases with time, as shown in Figure 19.

Interpretation of Chloride Threshold Concentrations for Initiation

The potentiostatic polarization/current monitoring method was chosen to investigate Cl⁻ threshold concentrations in order to eliminate problems such as the scan rate dependency of critical threshold potentials seen in potentiodynamic polarization methods. This effect is due to long
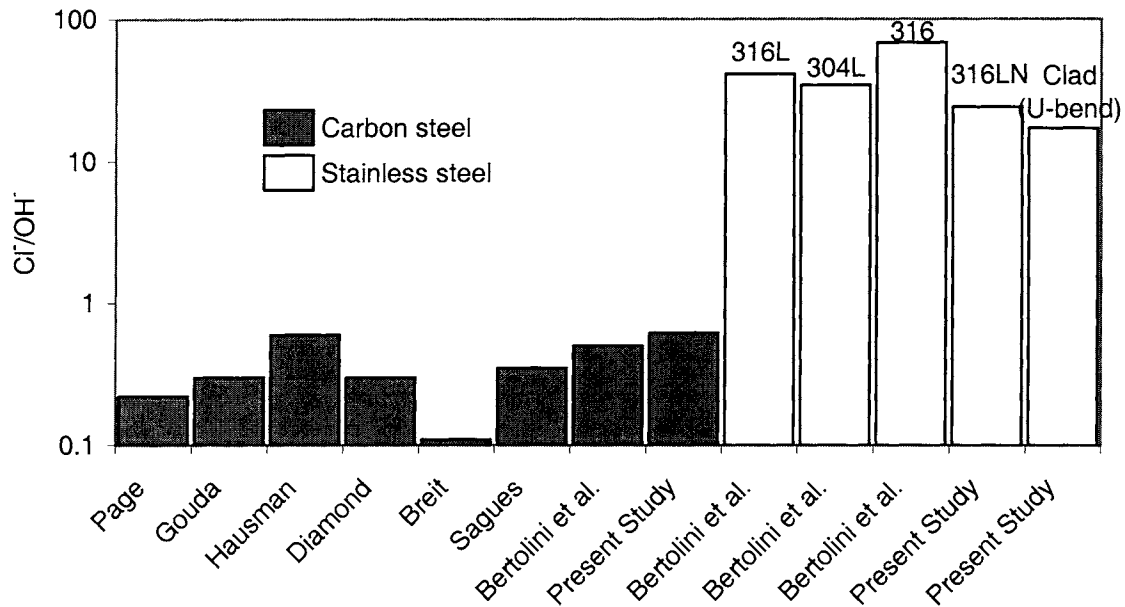
Figure 23. Literature reported Cl⁻/OH⁻ ratios for plain carbon steel and various grades of solid stainless steel. Results for solid 316LN and clad 316L (best value) obtained in this study at +0.2 V are on the far right. Carbon steel was tested in this study at –0.2 V, while the literature results for carbon steel were based on studies at the corrosion potential.

incubation times for corrosion initiation, which renders the scanning method ineffective. The 24-hour time period used before increasing the chloride concentration ensured that at least a short incubation time could be overcome in order to determine Cl⁻ thresholds, but longer term lab tests are still recommended. Nevertheless, a large difference is seen between the critical chloride initiation concentrations for carbon steel and stainless steel (Figure 23) in this study and in the literature (Bertolini et al., 1996). The results show that the chloride threshold concentration for corrosion initiation on stainless steel is much larger than for carbon steel. In addition, carbon steel suffered from more widespread attack (Figures 8 and 12), while corrosion on stainless steels initiated and grew at distinct pit sites (Figures 15 and 18).

The chloride threshold for 316L-clad rebar shows a strong dependence on the method and quality of sealing the exposed end (see Figure 17). Clad rebar with sealed ends often exhibited a low chloride threshold compared to solid 316LN stainless steel reflecting the quality of the seal at the cut end. The implication is that the poor seal allowed exposure of carbon steel, which possesses a lower chloride threshold at all potentials (Figure 9). Visual evidence of corrosion in the carbon steel core at the end of the test confirmed this hypothesis. The 316L-clad U-bend samples yielded chloride thresholds equal to that of the best case test for 316L-cladding with an epoxy-sealed end (e.g., Cl⁻/OH⁻ = 17). The chloride threshold was considerably higher than that of the carbon steel, yet not equal to that of solid 316LN stainless steel (e.g., Cl⁻/OH⁻ = 24). This difference could be due to the different compositions of the solid and clad stainless steels, as indicated by their respective PREN numbers. The solid 316LN stainless steel bar has a PREN number of 30.72, while the 316L-clad bar has a lower PREN of 24.15. Additionally, it was impossible to use the same electrochemical cell lid for the U-bend test as in the solid bar tests due to specimen geometry.

This led to more ready formation of a "skin" at the electrolyte/air interface around the rebar. Corrosion products and, possibly, salt deposits formed preferentially at the water line in U-bend chloride threshold determination tests. The salt deposits may have provided a more aggressive environment, conducive to local corrosion attack, that promoted the observed corrosion at a lower threshold chloride concentration than seen for straight bars of solid 316LN stainless steel. No such corrosion or significant skin formation was observed in the experiments with straight bars.

Stainless steel has a much higher chloride initiation threshold ($Cl^-/OH^- > 100$) than carbon steel ($Cl^-/OH^- \approx 1.5$) for tests conducted at 0 mV and –200 mV in saturated $Ca(OH)_2$ solutions. These results are likely conservative since the $Ca(OH)_2$ solution may be more aggressive than concrete (Glass and Buenfield, 2000). The chloride initiation threshold of solid 316LN and intact 316L-clad stainless steel at +200 mV decreased to a Cl^-/OH^- molar ratio ranging from >15 to about 24 (Figures 9,17, and 23). It is of interest to compare the OCP of the different rebars to the chloride threshold obtained at various potentials in order to determine which potential-dependent chloride threshold best describes the situation in concrete. The open circuit potentials of all materials before corrosion initiation are rising toward –50 mV over time (Figures 7 and 19). This substantiates the need for Cl^- threshold information over a range of applied potentials. A detrimental situation is created by exposure of stainless steel-clad rebar with a cut end that exposes the carbon steel core. Here the OCP can remain high compared to active carbon steel by itself due to galvanic coupling between the passive stainless steel-cladding and the exposed active carbon steel core. The chloride threshold reported here is for the active carbon steel core at elevated potentials while the stainless steel-clad layer remains unaffected.

Uncertainty over exact Cl^- threshold values arises from the long incubation times associated with initiation of local corrosion and the statistical distributions often seen in all thresholds for local corrosion. Recall that the Cl^- concentration is linked to electrochemical potential and should not be considered independent of potential as is the current practice of those in the highway transportation field. The critical potential for pitting and crevice initiation on stainless steels (E_{thres}) is a function of chloride concentration (Sedriks, 1996), as was seen earlier (Equations 2 and 3), as well as the time of exposure at a given applied potential. Therefore, Cl^- threshold and critical potentials are always linked. The higher the applied potential above the E_{thres} value obtained at long times for a given Cl^- concentration, the shorter the initiation time. Thus, potentiostatic holds at +200 mV likely enable valid determination of chloride threshold concentrations for 316L and 316LN stainless steel when NaCl is added in steps every 24 hours because the incubation period is overcome. Therefore, the chloride initiation threshold obtained in potentiostatic tests likely represents the condition when the applied potential (E_{app}) equals or slightly exceeds the long-term chloride-dependent critical threshold potential (E_{thres}) for chloride-induced pitting such as the pitting potential, E_{pit}. Localized corrosion likely occurred in potentiostatic tests at potentials very close to the condition: $E_{app} = E_{thres}$ because a 24-hour hold period at each Cl^- concentration provided enough time to overcome the incubation time associated with initiation. Figures 11 and 13 indicate that E_{pit} and E_r obtained from potentiodynamic scans are not reliable indicators of the Cl^- threshold for initiation of stainless steels because the passive film may not have broken down during the limited time of the scan (i.e., 30 min). In other words, scanning is an inappropriate method for determination of threshold Cl^- concentrations for stainless steels because of the need to overcome the incubation time associated with passive film breakdown. In contrast, the scanning method can be used for determination of

threshold Cl⁻ concentrations for plain carbon steel (Li and Sagues, 1999). One way to eliminate the incubation time associated with E_{thres} is to initiate local corrosion intentionally and study the repassivation potential, E_r. The usefulness of this parameter lies in the fact that the incubation time is eliminated.

The Chloride Concentration for Corrosion Suppression Determined by Abrupt Changes in E_r

The repassivation potential, E_r, represents the potential below which pits, even if initiated, will be repassivated. E_r provides several crucial pieces of information. First, E_r was much more positive for solid 316LN stainless steels than for carbon steel over a range of NaCl concentrations (Figure 10). E_r values for carbon steel were not associated with repassivation of a passive electrode containing isolated pits but were, instead, associated with the OCP of activated carbon steel. Hence, carbon steel never repassivated once local corrosion was initiated. This is a significant difference between these two materials.

Second, 316L-clad stainless steel had an E_r value equal to that of solid 316LN stainless steel as long as the clad layer was not penetrated (Figure 14). This is another metric that indicates that intact 316L-clad stainless steel is nearly equivalent to 316LN. Moreover, the lack of pit depth dependency on E_r (Figure 14) is consistent with the notion that the crevice formers present due to the glass beads and sand provide the critical dimension that controls mass transport in and out of the local corrosion site, not the depth of corrosion damage (Kelher et al., 2001). Therefore, E_r did not depend on depth of corrosion. When penetration occurred, E_r dropped to the low values near those associated with carbon steel (Figures 10 and 14). However, this occurred when the pit depth was greater than the clad thickness. Thus, in the rare instance that crevice attack occurs on the cladding and penetrates through to the carbon steel, the 316L-clad material would no longer be as corrosion resistant as solid 316LN stainless steel. Rapid attack of the carbon steel would be expected due to the more aggressive pit chemistry formed as a result of stainless steel crevice attack.

There is a critical potential associated with initiation and one associated with repassivation, E_r (Sedriks, 1996). Likewise there will be a critical Cl⁻ concentration associated with initiation of corrosion and one below which repassivation or suppression of corrosion will occur. A chloride threshold value for initiation of pitting on 316LN stainless steel, expressed as a Cl⁻/OH⁻ molar ratio of about 24, was found to initiate localized corrosion (at +200 mV) on solid 316LN stainless steel. A Cl⁻/OH⁻ value below 0.4 was found to be a corrosion suppression threshold for solid 316LN (Figures 10 and 13). It is associated with the chloride level where an abrupt increase in E_r was observed. Pits or crevices, even if formed, would repassivate at this Cl⁻/OH⁻ molar ratio. Therefore, this represents a true corrosion suppression threshold for Cl⁻-induced attack of stainless steel. In contrast, corrosion remained active, once initiated, on carbon steel at all Cl⁻/OH⁻ molar ratios tested here (Figures 10 and 11). Hence, a true chloride threshold concentration, below which corrosion is suppressed, does not exist for carbon steel in these short-term lab tests.

Galvanic Corrosion between 316L Cladding and Exposed Plain Carbon Steel Core

Galvanic corrosion on stainless steel-clad rebar may occur at any physical breach in the stainless steel-clad layer exposing the carbon steel core. However, Figure 22 indicates that galvanic corrosion rates will be severe only when the chloride threshold for carbon steel is exceeded. That is because galvanic corrosion requires a difference in OCP between the metals forming the galvanic couple, and this is not seen in Figure 7. However, galvanic attack is expected when the Cl⁻ threshold is exceeded for carbon steel, as indicated by the differences in OCP values shown in Figure 7 when plain carbon steel is activated. Upon such conditions, it is expected that the corrosion rate of active carbon steel rebar would be accelerated as shown in Figure 22 and the OCP would lie somewhere between that of passive stainless steel and active carbon steel. The condition would be exacerbated with increasing cathode to anode areas as shown in Figure 22.

The corrosion rate of the exposed core on imperfect clad rebar depends highly on the geometry of the setup and conductivity of the surrounding media. For example, a nick in the cladding (exposing a very small area of the core) would have a very large cathode to anode area ratio, while a cut-end clad bar (exposing a larger transverse section of the carbon steel core) in low conductivity concrete will have a smaller cathode to anode area ratio. This is because anodic areas at defects in stainless steel-cladding are, in practice, galvanically coupled only to passive stainless steel regions from which current can be thrown. Throwing power defines the size of the cathode that participates. However, as cathode area increases so does the ohmic resistance between physically separated anodes and cathodes. As ohmic potential (iR_Ω) increases, the cathodic and anodic overpotentials ($\eta_{cathode}, \eta_{anode}$) become smaller as governed by Equation 8.

$$\Delta E_{galvanic} = E_{corr}(\text{cathode}) - E_{corr}(\text{anode}) = \Sigma|\eta_{cathode}| + \Sigma\eta_{anode} + iR_\Omega \quad (8)$$

This leads to a lowering of the galvanic corrosion current and places a limit on the amount of cathode area that can participate. At greater distances away from anodic areas, the ohmic resistance associated with concrete becomes so large that the area becomes shielded from participating in galvanic corrosion. The results of this study indicate that 1000/1 cathode/anode area ratios are possible and reasonable to consider, as done in Figure 22.

Mechanical Damage

The sharp rise in the galvanic couple potential in the case of a mechanical defect (Figure 22) is due to the fact that carbon steel at Cl⁻/OH⁻ = 0.4 (0.01 M NaCl) exhibits passive corrosion behavior and the intersection of the cathodic E-log(i) curve for stainless steel curve occurs in the passive region of the anodic E-log(i) curve for carbon steel. This occurs when the chloride threshold for carbon steel has not been reached. The significant result is that there will not be galvanic corrosion when carbon steel is exposed under these conditions. However, when tested above the threshold (Cl⁻/OH⁻ = 4, 0.1 M NaCl), the galvanic couple potential does not rise as much as in the passive case due to the faster anodic kinetics and lower OCP associated with actively corroding carbon steel. Galvanic corrosion rates are accelerated for the carbon steel and can be increased by two orders of magnitude at high cathode/anode area ratios (Figure 22).

Corrosion Damage

When the carbon steel is exposed by corrosion, the galvanic corrosion rate was increased compared to the case of mechanical damage (figure not shown). This is explained by the presence of a more severe local environment at corrosion-induced damage sites; thus the carbon steel corrodes at a faster rate at each applied potential since it is no longer passive. However, stainless steel crevice attack is rare and occurs at discrete sites. Therefore, there would be very few sites for such galvanic attack.

Influence of Chloride Threshold Concentration on Relative Initiation Time

Given the difference in chloride initiation and suppression thresholds between plain carbon steel and solid stainless steel rebars, it is possible to create a model of the relative extension of the initiation phase for active corrosion afforded by using stainless steel instead of carbon steel. This model is based on Fickian diffusion of chloride into concrete. Given the increase in chloride initiation threshold expressed as a Cl^-/OH^- molar ratio from 1 to 4 for plain carbon steel to a Cl^-/OH^- molar ratio of 24 to 100 for solid stainless steel, the following question can be asked. How long does it take for the Cl^-/OH^- molar ratio in the concrete pore solution adjacent to an embedded rebar to reach the chloride initiation thresholds described? A calculation can be performed to estimate time until initiation, assuming diffusion of Cl^- into concrete to the depth of the rebar from the concrete surface by purely concentration gradient driven diffusion (Bentour et al., 1997; Kurtis and Mehta, 1997; Berke and Hicks, 1992; Cady and Weyers, 1992; Andrade and Alonso, 1996). Using a mathematical solution to Fick's second law of diffusion yields Equation 9, which describes the chloride concentration as a function of depth and time, assuming a constant surface concentration and transport into a semi-infinite medium.

$$C(x,t) = C_o \bullet \{1 - erf[x / (D_{eff} \bullet t)^{1/2}]\} \tag{9}$$

Here $C(x,t)$ is the chloride concentration at depth x and time t; C_o is the surface concentration; and D_{eff} is the effective diffusion coefficient. The inputs for the model must be chosen carefully since the output can vary greatly with C_o and D_{eff}. Such a relative calculation has been performed assuming relatively high and low D_{eff} and C_o values and a suitable standard concrete cover of 5 cm (Bentour et al., 1997) (see Figure 24). The accuracy of these calculations may be limited due to the lack of an accurate D_{eff} and uncertainty in estimation of the surface concentration (C_o) (Bentour et al., 1997; Kurtis and Mehta, 1997; Berke and Hicks, 1992; Cady and Weyers, 1992; Andrade and Alonso, 1996). D_{eff} varies with Cl^- concentration, concrete age, concrete quality, and external conditions, such as weather and concrete cracking (Cady and Weyers, 1992). A D_{eff} of 3×10^{-8} cm^2/s is appropriate for high quality concrete (w/c = 0.4) at a temperature of 22 °C (Bentour et al., 1997). The actual value of C_o depends on environmental conditions and varies with time in real exposures involving intermittent salt applications. Moreover, an exact calculation of the corrosion initiation time can not be made because of the variability in road salt deposition and rainfall from one location to another. Therefore, it is difficult to say exactly how long the corrosion initiation phase would be extended in service with the use of stainless steel rebar. Nevertheless, the calculations show that the use of defect-free stainless steel-clad rebar could significantly extend the time until initiation of chloride-induced

corrosion. For example, under even the mildest conditions (lowest C_0, slowest D_{eff}) shown in Figure 24, the chloride threshold concentration for corrosion initiation on carbon steel is exceeded in less than 8 years, while under many scenarios the chloride threshold for corrosion initiation on stainless steel has not been exceeded after 100 years. Hence, a relative increase in initiation time of > 10 may be achieved through use of intact 316L-clad stainless steel. Calculations with more realistic, variable, surface chloride concentrations representative of chloride deposition and removal by rainfall might be even more optimistic.
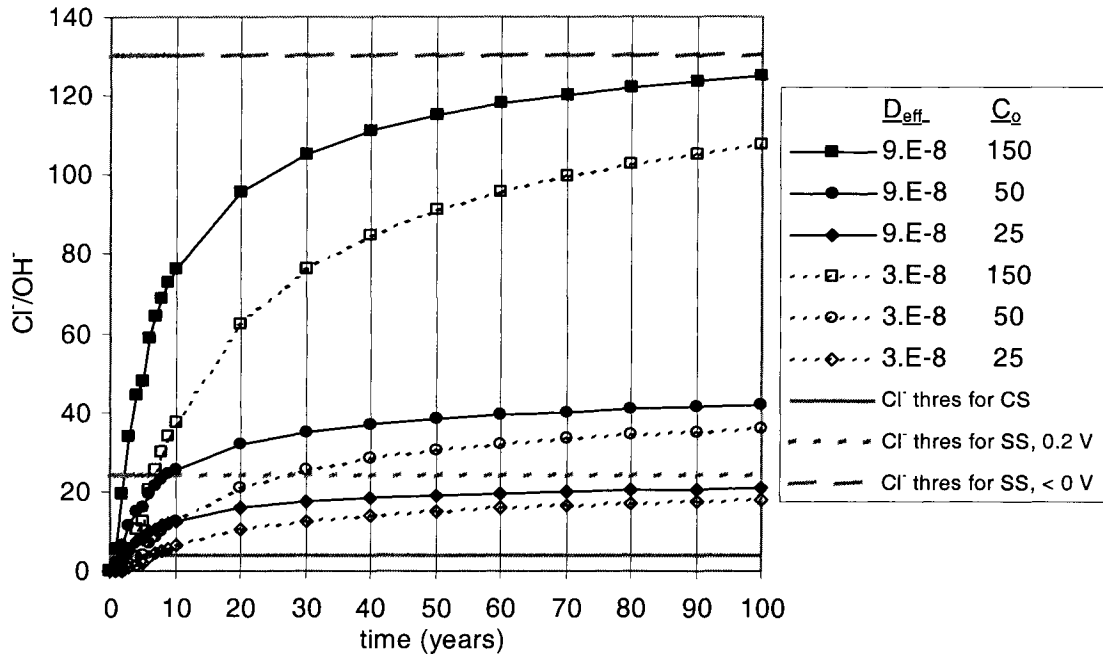

Figure 24. Cl^-/OH^- ratios at a depth of 5 cm in concrete versus time in years calculated from Equation 9 for various indicated values for D_{eff} (cm²/s) and C_0 (expressed as Cl^-/OH^-). Cl^- corrosion initiation threshold concentrations are shown for the best case plain carbon steel ($Cl^-/OH^- = 4$), for solid 316LN stainless steel (+200 mV, $Cl^-/OH^- = 24$), and for intact (defect free) stainless steel (-200 to 0 mV), at an assumed $Cl^-/OH^- \geq 130$ (>NaCl saturation limit).

CONCLUSIONS

• In this study, the potentiostatic method was used to determine the chloride thresholds for corrosion initiation of plain carbon steel rebar in simulated pore solution in laboratory tests. A Cl^-/OH^- molar ratio less than 1.5 was obtained. There is a consensus that the threshold for carbon steel lies below a Cl^-/OH^- molar ratio of 4 for tests conducted in concrete and below a Cl^-/OH^- molar ratio of 1.5 for tests conducted in simulated pore solutions. There is good agreement between chloride threshold concentrations obtained for carbon steel from several different methods. Methods that can be used include R_p, E_{corr}, potentiostatic holds, and potentiodynamic polarization scans.

• Concerning 316L-clad and 316LN solid stainless steel, the potentiostatic polarization method was found to be an effective means to determine chloride thresholds for corrosion initiation.

40

Other methods such as potentiodynamic polarization scans did not provide an effective means to determine chloride threshold concentrations for corrosion initiation in simulated pore solution in short-term laboratory tests.

- At -200 and 0 mV vs. SCE, the chloride threshold for corrosion initiation of solid 316LN stainless steel was conservatively placed at the saturation point of NaCl (Cl^-/OH^- molar ratio $\geq$ 100) in saturated $Ca(OH)_2$. Corrosion had not been initiated at this point after 24 h exposure in laboratory tests, but further increasing the chloride concentration was not possible due to saturation. At $+200$ mV, the chloride thresholds for corrosion initiation, expressed as a Cl^-/OH^- molar ratio, were found to be as high as 24 for solid stainless steel.

- Intact 316L-clad stainless steel rebar specimens possessed similar electrochemical corrosion properties (e.g., E_{OCP}, E-log(i), and pit repassivation potentials, E_r) as solid stainless steel counterparts. The chloride thresholds for corrosion initiation of intact 316L-clad stainless steel rebar specimens, expressed as a Cl^-/OH^- molar ratio, was also found to average 16 and be as high as 17. However, the highest recorded chloride initiation threshold for intact 316L stainless steel-clad rebar specimens was not as high as that for solid 316LN stainless steel. This was attributed to differences in alloy composition.

- The chloride thresholds for corrosion initiation of 316L stainless steel-clad rebar specimens, expressed as a Cl^-/OH^- molar ratio, decreased toward the results for plain carbon steel when cut ends, ineffectively welded ends, and ineffectively sealed epoxy ends were exposed in $Ca(OH)_2$ + NaCl solutions. Hence, the chloride threshold for corrosion initiation on stainless steel-clad rebar was found to be strongly dependent on the method of covering the carbon steel core at the cut end of the rebar. At best, the chloride threshold is similar to that of solid stainless steel rebar, but when the cut end exposes plain carbon steel, the chloride threshold was equal to that of carbon steel.

- Repassivation potential, E_r, values provided an additional metric for comparison of solid and stainless steel-clad rebar to plain carbon steel. E_r values for 316L-clad stainless steel were equivalent to solid 316LN stainless steel as long as the stainless steel-clad layer had not been penetrated by corrosion attack.

- A new parameter was discovered and reported. It is the critical Cl^- concentration in a simulated pore solution below which corrosion, once initiated, would be suppressed. This was termed the chloride concentration for corrosion suppression. A distinct critical Cl^- concentration for corrosion suppression was found for 316LN stainless steel where E_r increased far above E_{OCP}. In contrast, no abrupt increase in repassivation potential was observed for carbon steel at Cl^-/OH^- molar ratios as low as 0.04. Thus, a chloride concentration for corrosion suppression of carbon steel could not be defined in short-term laboratory tests.

- Galvanic coupling between cladding and carbon steel cores, due to defects in the 316L-clad stainless steel bar that expose the carbon steel core, was found to be detrimental to the corrosion performance of clad rebar with a physical penetration only in chloride solutions.

Corrosion was accelerated on physically exposed carbon steel cores only when it was exposed in a $Ca(OH)_2 + NaCl$ solution above the chloride initiation threshold for corrosion of carbon steel. Increasing the cathode to anode area ratio caused progressively greater galvanic couple potentials and galvanic corrosion rates. In contrast, exposure of physically exposed carbon steel in chloride-free $Ca(OH)_2$ solutions did not result in galvanic corrosion. Galvanic corrosion was also accelerated when carbon steel was exposed by electrochemical penetration of the stainless steel-cladding.

- Since intact stainless steel-clad rebar possesses nearly equally high resistance to initiation of chloride-induced corrosion as obtained with solid stainless steel 316LN, its use can lead to significant lifetime extensions for concrete structures due to improved chloride threshold concentrations compared to carbon steel. Fickian diffusion calculations with fixed surface chloride concentration show that the increased chloride threshold of defect-free stainless steel rebar may increase, by orders of magnitude, the time until initiation of chloride-induced corrosion over that for carbon steel. Calculations with more realistic, variable, surface chloride concentrations might be even more optimistic.

RECOMMENDATIONS

- Since the stainless steel–clad bar evaluated in this project can extend the service life of concrete bridges, it should be used in the construction of new concrete bridges.

- Further study should be dedicated to effective sealing methods for the cut ends of clad rebar materials in order to gain the full benefit of intact clad rebar. Ineffective sealing of cut ends can reduce the time until corrosion initiation because chloride thresholds are reduced. However, the effects of corrosion propagation at such spatially discrete sites on eventual concrete damage by corrosion product wedging are unclear, since corrosion damage starts at the cut end and would require delamination of the cladding prior to spreading across a large surface area of the reinforcing bar.

- Chloride thresholds for solid and stainless steel-clad rebar should be confirmed over longer time periods than the 24 h used in these laboratory tests. Moreover, additional fine increments in chloride levels should be tested that will lead to more narrowly defined chloride thresholds. Also, research needs to be conducted into the statistical spread of the chloride threshold results on all types of rebars. This consists of running multiple tests under the potentiostatic polarization condition to illuminate scatter, effects of surface preparation, and effects of different cut-end sealing preparation methods (specific to the clad rebar). Tests should be conducted in simulated concrete (as opposed to actual concrete or mortars) because of the relative ease of obtaining conservative results, as this study has shown.

- The identity and specific volume of the corrosion products on new rebar materials must be examined and determined. The risk of concrete damage due to corrosion product wedging will depend on the properties of the corrosion products as well as the depth and area of corrosive attack. Regarding the latter, the morphology of corrosion damage in carbon steel and 316L or

316LN stainless steel was very different. Corrosion damage may occur to greater depths and over larger regions of the rebar in the case of carbon steel. Experiments should be conducted utilizing electrode arrays to monitor the spread of corrosion across the rebar surface once initiated. An added benefit of stainless steels would be a reduced area of attack, as the corrosion pitting morphology in this study indicates.

- The corrosion propagation properties on new rebar materials must also be further investigated to fully understand the benefits of corrosion-resistant rebar during the propagation stage as well as the initiation stage. Testing conducted in concrete would supplement results from testing conducted in simulated concrete.

REFERENCES

Allen, J. Epoxy-Coated Rebar Benefits Minnesota Decks. *Road and Bridges,* Vol. 38, June 1993, p. 38.

Alonso, C., Andrade, C., Castellote, M., and Castro, P. Chloride Threshold Values to Depassivate Reinforcing Bars Embedded in a Standardized OPC Mortar. *Cement and Concrete Research,* Vol. 30, No. 7, July 2000, pp. 1047-1055.

Andrade, C., and Alonso, C. Progress on Design and Residual Life Calculation with Regard to Rebar Corrosion of Reinforced Concrete. In *Techniques to Assess the Corrosion Activity of Steel Reinforced Concrete Structures.* American Society for Testing and Materials. Philadelphia, 1996.

Andrade, C., and Page, C. L. Pore Solution Chemistry and Corrosion in Hydrated Cement Systems Containing Chloride Salts: A Study of Cation Specific Effects. *Cement and Concrete Research,* Vol. 21, 1986, pp. 49-53.

ASTM C114-83a, Standard Method for Chemical Analysis of Hydraulic Cement. American Society for Testing and Materials, Philadelphia, 1983.

Bentour, A., Diamond, S., and Berke, N. *Steel Corrosion in Concrete.* E & FN Spon, London, 1997.

Berke, N. S., and Hicks, M. C. Estimating the Life Cycle of Reinforced Concrete Decks and Marine Piles Using Laboratory Techniques. In *Corrosion Forms and Control for Infrastructure.* American Society for Testing and Materials, Philadelphia, 1992.

Bertolini, L., Bolzoni, F., Pastore, T., and Pedererri. P., Behaviour of Stainless Steel in Simulated Concrete Pore Solution. *British Corrosion Journal,* Vol. 31, No. 3, 1996, pp. 218-222.

BS 1881: Part 124. British Standard Specification for the Testing of Hardened Concrete. British Standards Institution, London, 1988.

Burnstein, G. T., and Ilevbare, G. O. The Effect of Specimen Size on the Measured Pitting Potential of Stainless Steel. *Corrosion Science,* Vol. 38, No. 12, December 1998, pp. 2257-2265.

Cady, P. D., and Weyers, R. E. Predicting Service Life of Concrete Bridge Decks Subject to Reinforcement Corrosion. In *Corrosion Forms and Control for Infrastructure.* American Society for Testing and Materials, Philadelphia, 1992.

Clear, K. C. Effectiveness of Epoxy-Coated Reinforcing Steel (C-SHRP Report: Executive Summary). In *Transportation Research Circular,* Vol. 403, 1996, p. 66.

Cox, R. N., and Oldfield, J. W. The Long Term Performance of Austenitic Stainless Steel in Chloride Contaminated Concrete. In *Corrosion of Reinforcement in Concrete Construction,* The Royal Society of Chemistry, London, 1996, pp. 662-669.

Dunn, D., and Sridhar, N. *Investigation of Processes Related to the Growth and Repassivation of Localized Corrosion of Fe-Ni-Cr-Mo Alloys,* Presented at the Electrochemical Society, 1995.

Feliu, S., Gonzalez, J. A., Feliu, S. Jr., and Andrade, C. Relationships Between Conductivity of Concrete and Corrosion of Reinforcing Bars. *British Corrosion Journal,* Vol. 24, No. 3, 1989, pp. 195-198.

Glass, G. K., Hassanein, N. M., and Buenfield, N. R. Neural Network Modeling of Chloride Binding. *Magazine of Concrete Research,* Vol. 49, No. 181, December 1997, pp. 323-335.

Glass, G. K., and Buenfield, N. R. The Presentation of the Chloride Threshold Level for Corrosion of Steel in Concrete. *Corrosion Science,* Vol. 39, No. 5, May 1997, pp. 1001-1013.

Glass, G. K., and Buenfield, N. R. The Influence of Chloride Binding on the Chloride Induced Corrosion Risk in Reinforced Concrete. *Corrosion Science,* Vol. 42, No. 2, February 2000, pp. 329-344.

Goni, S., and Andrade, C. Synthetic Concrete Pore Solution Chemistry and Rebar Corrosion Rate in the Presence of Chlorides. *Cement and Concrete Research,* Vol. 20, No. 4, July 1990, pp. 525-539.

Gouda, V. K. Corrosion and Inhibition of Reinforcing Steel. *British Corrosion Journal*, Vol. 5, 1970, pp. 198-203.

Gouda, V. K., and Halaka, W. Y. Corrosion and Corrosion Inhibition of Reinforced Steel. *British Corrosion Journal*, Vol. 5, 1970, pp. 204-208.

Hansson, C. M., and Sorensen, B. *The Threshold Concentration of Chloride in Concrete for Initiation of Reinforcement Corrosion.* In Corrosion Rates of Steel in Concrete, American Society for Testing and Materials, Philadelphia, 1992.

Hausmann, D. A. Steel Corrosion in Concrete. How Does it Occur? *Journal of Materials Protection*, Vol. 11, 1967, pp. 19-23.

Hope, B. B., and Ip, A. K. C. Corrosion and Electrical Impedance in Concrete. *Cement and Concrete Research*, Vol. 15, 1985, pp. 525-534.

Hope, B. B., and Ip, A. K. C. Chloride Corrosion Threshold in Concrete. *ACI Materials Journal*, Vol. 84, No. 4, July-August 1987, pp. 306-314.

Hurley, M. F. *Critical Issues Regarding the Corrosion Behavior of Stainless Steel-Clad Rebar.* University of Virginia, Charlottesville, 2002.

Hussain, S. E., Rasheduzzafar, A., Al-Mussallam, A., and Al-Gahtani, A. Factors Affecting Threshold Chloride for Reinforcement Corrosion in Concrete. *Cement and Concrete Research*, Vol. 25, No. 7, October 1995, pp. 1543-1555.

Jones, D. A. *Principals and Prevention of Corrosion.* Prentice-Hall, Inc., Upper Saddle River, NJ, 1996.

Kayyali, O. A., and Haque, M. N. The Ratio of Cl⁻/OH⁻ in Chloride Contaminated Concrete. A Most Important Criterion. *Magazine of Concrete Research*, Vol. 47, No. 172, September 1995, pp. 235-242.

Kehler, B. A., Ilevbare, G. O., and Scully, J. R. *Crevice Corrosion Stabilization and Repassivation Behavior of Alloys 625 and C22*, Presented at Corrosion 2001, National Association of Corrosion Engineers, Houston, 2001.

Kurtis, K. E., and Mehta, K. A. *Critical Review of Deterioration of Concrete Due to Corrosion of Reinforcing Steel.* Presented at Fourth CANMET/ACI International Conference on Durability of Concrete, Sydney, Australia, 1997.

Lambert, P., Page, C. L., and Vassie, P. R. W. Investigation of Reinforcement Corrosion. Electrochemical Monitoring of Steel in Chloride Contaminated Concrete. *Materials Structure*, Vol. 24, No. 143, September 1991, pp. 351-358.

Li, L., and Sagues, A. A. *Effect of Chloride Concentration on the Pitting and Repassivation Potentials of Reinforcing Steel in Alkaline Solutions*. Presented at Corrosion '99, National Association of Corrosion Engineers, Houston, 1999.

Li, L., and Sagues, A. A. Chloride Corrosion Threshold of Reinforcing Steel in Alkaline Solutions-Open-Circuit Immersion Tests. *Corrosion*, Vol. 57, No. 1, January 2001, pp. 19-28.

Macdonald, D. D., McKubre, M. C. H., and Urquidi-MacDonald, M. Theoretical Assessment of AC Impedence Spectroscopy for Detecting Corrosion of rebar in Reinforced Concrete. *Corrosion*, Vol. 44, No. 1, January 1988, pp. 2-7.

Mehta., P. K. *Concrete Structure, Properties, and Materials*. Prentice-Hall, Inc., Englewood Cliffs, NJ, 1986.

Nawy, E. G. *Reinforced Concrete: A Fundamental Approach*. Prentice Hall, Inc., Upper Saddle River, NJ, 2000.

Nurnberger, U., Ed. *Stainless Steel in Concrete*. The Institute of Materials, London, 1996.

Participant Workbook. Strategic Highway Research Program, Washington, D.C., 1985.

Petterson, K. H. Chloride Threshold Value and the Corrosion Rate in Reinforced Concrete. *Proceedings of the International Conference on Corrosion Protection of Steel in Concrete*, Swamy, R. N., Ed., Academic Press, Sheffield, 1994, p. 461.

Petterson, K. H. Factors Influencing Chloride Induced Corrosion of Reinforcement in Concrete. *Durability of Building Materials and Components*, Sjostrom, C., Ed., Vol. 1. Chapman & Hall, London, 1996, pp. 334-341.

Petterson, K. H. *Chloride Threshold Value and the Corrosion Rate in Reinforced Concrete*. Report 2:92. Swedish Cement and Concrete Research Institute, Stockholm, 1992.

Pourbaix, M. *Atlas of Electrochemical Equilibria in Aqueous Solutions*. National Association of Corrosion Engineers, Houston, TX, 1974.

Rosenberg, A., Hansson, C. M., and Andrade, C. Mechanisms of Corrosion of Steel in Concrete. *Materials Science of Corrosion I*, The American Ceramic Society, Waterville, OH, 1989.

Schiessl, P., and Breit, W. *Local Repair Measures at Concrete Structures Damaged by Reinforcement Corrosion*. The Fourth International Symposium on Corrosion of Reinforcement in Concrete Construction, Cambridge, 1996.

Sedriks, J. A. *Corrosion of Stainless Steels*. John Wiley & Sons, Inc., Princeton, NJ, 1996.

Shibata, T., and Takeyama, T. Stochastic Theory of Pitting Corrosion. *Corrosion*, Vol. 33, No. 7, July 1977, pp. 243-251.

Smith, L. L., Kessler, R. J., and Powers, R. G. Corrosion of Epoxy-Coated Rebar in a Marine Environment. *Transportation Research Circular*, Vol. 403, 1993, p. 36.

Sohanghpurwala, A., and Scannell, W. T. *Field Performance of Epoxy-Coated Reinforcing Steel in the States of Pennsylvania and New York.* Presented at the 77th Annual Meeting of the Transportation Research Board, Washington, DC, 1998.

Szlarska-Simialowska, Z. *Pitting Corrosion of Metals.* National Association of Corrosion Engineers, Houston, TX, 1986.

Thomas, M. D. A., Matthews, J. D., and Haynes, C. A. Chloride Diffusion and Reinforcement Corrosion in Marine Exposed Concretes Containing PFA. *Corrosion of Reinforcement in Concrete.* Page, C. L., Treadway, K. W. J., and Bamforth, P. B., Eds., Elsevier, Warwickshire, UK, 1990, pp.198-212.

Thomas, M. Chloride Thresholds in Marine Concrete. *Cement and Concrete Research*, Vol. 26, No. 4, April 1996, pp. 513-519.

Thompson, N. G., and Syrett, B. C. Relationship Between Conventional Pitting and Protection Potentials and a New, Unique Pitting Potential. *Corrosion*, Vol. 48, No. 8, August 1992, pp. 649-659.

Tonini, D. E., and Gaidis, J. M., Eds. *Corrosion of Reinforcing Steel in Concrete.* American Society for Testing and Materials, Philadelphia, 1980.

Tuutti, K. *Corrosion of Steel in Concrete.* Swedish Cement and Concrete Research Institute, Stockholm, 1982.

Uhlig, H. H., and Greene, N. D. *Corrosion and Corrosion Control.* Wiley, New York, 1985.

USDOT, *Corrosion Evaluation of Epoxy-Coated, Metallic-Clad and Solid Metallic Reinforcing Bars in Concrete.* Federal Highway Administration, McLean, VA, 1998.

Wilde, B. E. A Critical Appraisal of Some Popular Laboratory Electrochemical Tests for Predicting the Localized Corrosion Resistance of Stainless Alloys in Sea Water. *Corrosion*, Vol. 28, No. 8, August 1972, pp. 283-291.

Yonezawa, T., Ashworth, V., and Procter, R. P. M. Pore Solution Composition and Chloride Effects on the Corrosion of Steel in Concrete. *Corrosion*, Vol. 44, No. 7, July 1988, pp. 489-499.

Zimmerman, L., Elsener, B., and Bohni, H. Critical Factors for the Initiation of Rebar Corrosion. In *Eurrocorr '99 Proceedings*. Dechema, Frankfurt, 1999, p. 239.